Supporting Information

Cr–O–In Interlocking for Window Layer Delamination Resistance in Operationally Stable Perovskite/Silicon Tandem Solar Cells

Huan Li[1], Zhiqin Ying[1,*], Wenfeng Liu[1,3], Xin Li[1], Fanshu Kong[1], Ziyu He[1], Haofan Ma[1], Yunyun Yu[1], Rui Li[1], Meili Zhang[1], Yan Zheng[1], Xuefeng Hu[1], Yuheng Zeng[1], Luyao Zheng[1], Xi Yang[1,2,*] and Jichun Ye[1,2,*]

[1]Ningbo Institute of Materials Technology and Engineering, Chinese Academy of Sciences (CAS), Ningbo, 315201, China

[2]Yongjiang Laboratory, Ningbo, Zhejiang, 315201, China

[3]School of Energy Science and Engineering, Central South University, Changsha 410083

*Corresponding author: Zhiqin Ying; Xi Yang; Jichun Ye; Email: yingzhiqin@nimte.ac.cn; yangx@nimte.ac.cn; jichun.ye@nimte.ac.cn

Methods

Materials

Anhydrous dimethyl sulfoxide (DMSO), dimethylformamide (DMF), isopropanol (IPA), chlorobenzene (CB) and cesium iodide (CsI) were purchased from Sigma-Aldrich. Lead iodine (PbI_2), lead bromide ($PbBr_2$) and 4-(7H-dibenzo[c,g]carbazol-7-yl)butyl) phosphonic acid (4PADCB) were purchased from TCI. Formamidinium iodide (FAI), methylammonium chloride (MACl) and methylammonium bromide (MABr) were purchased from Greatcell Solar Ltd. 1,3-Diaminopropane dihydroiodide ($PDAI_2$) was purchased from Xi'an Polymer Light Technology. Fullerene (C_{60}) and bathocuproine (BCP) were purchased from Taiwan Lumtec Corp. Tetrakis(dimethylamino)tin (IV) (TDMASn) (99.99%-Sn, Strem Chemicals) as one precursor of SnO_X was purchased from MNT Micro and Nanotech. All chemicals were purchased and used directly without further purification.

Device fabrication

For the wide-bandgap perovskite solar cells, the precursor solution with the concentration of 1.4 M was prepared by dissolving CsI, FAI, MABr, MACl, PbI_2 and $PbBr_2$ in 1 mL of a mixed solvent including DMF and DMSO with a volume ratio of 4:1. The perovskite composition is $Cs_{0.05}FA_{0.8}MA_{0.15}Pb(I_{0.76}Br_{0.24})_3$. The precursor solution was vibrated overnight and filtered using a 0.22 μm filter before the deposition. For perovskite devices, the glass/indium tin oxide (ITO) substrates with the size of 2.5 cm × 2.5 cm were sequentially cleaned in detergent water, distilled water and IPA using ultra-sonication for 30 min, respectively. All substrates were further treated with UV-ozone cleaner for 30 min. 80 μL of 4PADCB (0.5 mg mL^{-1}) was spin-coated on the cleaned ITO substrates at 3000 rpm for 30 s and annealed at 100 °C for 10 min. 80 μL perovskite precursor was spin-coated on the ITO/4PADCB film at 5000 rpm for 45 s. During the spin-coating process, 300 μL CB was immediately dropped on the center of spinning substrates at 10 s before finishing the program. The perovskite films were

annealed at 105 °C for 15 min. Subsequently, 60 μL of $PDAI_2$ (1.5 mg mL^{-1}) was dynamically spin-coated onto the perovskite film at a spinning rate of 5000 rpm for 30 s and annealed at 100 °C for 5 min. Then, the films were transferred to thermal evaporation equipment to deposit the electron transport layer of C_{60} (15 nm) layer. It is noted that the PVK/C_{60} film is exposed to ambient air during transfer to the ALD chamber. The buffer layer of SnO_X films deposited by an atomic layer deposition (ALD) technique at 80 °C in a chamber using an ALD cycle of TDMASn (at 70 °C)/Ar purge/H_2O (at 25 °C)/Ar purge with the pulse time of 0.2/15/0.1/15 s. High-purity Ar was used as carrier gas and purge gas. After that, the Ag electrode (90 nm) was thermally evaporated. For target devices, the SnO_X films were substituted by the thermal evaporation of Cr metal buffer layer (3 nm) under a low vacuum. The evaporation deposition chamber was pumped until the vacuum degree dropped to 10^{-4} torr. And the deposition rate of Cr film was controlled at 0.3-0.5 Å/s. No other annealing processes were utilized.

For the perovskite/silicon tandem solar cells, the TOPCon silicon bottom cells with 1 cm^2 active area were implemented as the bottom subcells. A 10 nm-thick indium zinc oxide (IZO) front recombination layer was prepared by via radio frequency magnetron sputtering with a RF power of 30 W and then annealed at 280 °C for 20 min, which can recover the sputtering damage. For perovskite top cell, the silicon bottom cell was UV-ozone cleaned for 15 min to increase the absorption density of 4PADCB. Then, the silicon substrates were transferred into a N_2-filled glovebox. The preparations of 4PADCB, perovskite film, surface passivation, C_{60}, SnO_X, Cr film were same as that of the single-junction perovskite solar cells. After deposition of SnO_X or Cr film, a 70 nm-thick IZO (sheet resistance of 100-150 Ω/sq) transparent electrode was deposited via radio frequency magnetron sputtering at room temperature with a RF power of 80 W. Finally, 300 nm U-shaped Ag electrode at a rate of 0.5-1.2 Å/s, 100 nm MgF_2 at a rate of 0.5-1.0 Å/s were thermally evaporated through a shadow mask, respectively.

Film characterization

The X-ray diffraction (XRD) patterns were obtained in air by using Bruker-D8 ADVANCE DAVINCI equipped with the Cu Kα radiation (λ = 1.5418 Å). The roughness and surface potential of perovskite films were collected from the kelvin probe atomic force microscope (KPFM) (Bruker, Dimension ICON). The conductive atomic force microscope (C-AFM) was measured by Bruker Nano Inc (Dimension ICON). The high-resolution scanning electronic microscope (SEM) images were acquired from Hitachi S4800 at an acceleration voltage of 4 kV and a current of 10 μA. The scanning transmission electron microscopy (STEM) was conducted by using an aberration-corrected FEI Titan Cubed Themis G2 operated at 300 kV, equipped with an XFEG gun and Bruker Super-X EDS detectors. The element distribution was captured in the STEM through the EDX software. The photoluminescence (PL) spectra and time-resolved PL (TRPL) were conducted by using an Edinburgh Instrument FLS1000 system applying a 450 nm laser as the excitation source. PL mapping was carried out with a laser confocal Raman spectrometer (KEYENCE, VK-X200K). The PLIM mapping measurement was conducted to obtain lifetime mapping spectra. The X-ray photoelectron spectroscopy (XPS) was conducted by using a multifunctional photoelectron spectrometer (Axis Ultra DLD, Kratos Analytical Ltd.) with Al Kα radiation (1486.7 eV) as an excitation source. For depth profile XPS analyses, a two-stage Ar cluster ion etch was used for depth profiling in **Figures 2f** and **2g**: first with Ar_{150}^+ at 6 keV in 10-second steps (to 90 s total), followed by Ar_{75}^+ at 8 keV in 30-second steps (from 120 s to 360 s total). For depth profiling in **Figure S11**, Argon ions sputtering was performed at 2 keV using a 2 mm × 2 mm raster scan by steps of 10 s (0-40 s), 30 s (70-190 s) and 120 s, respectively. Ar^+ etching proved to be significantly more effective for this sample. Clearly, the material removed in just the first 0-40 s of monoatomic etching corresponds to the depth achieved after over 300 s of cluster ion etching. The ultra-violet photoelectron spectroscopy (UPS) was conducted by the same

equipment as XPS while using monochromatized He I radiation at 21.22 eV. Time-of-flight secondary-ion mass spectrometry (ToF-SIMS) was carried out by a PHI nano TOF II TOF-SIMS (ULVAC-PHI, Japan) system. During the data acquisition, a pulsed 30 keV Bi_1^+ as primary ion beam was used to generate the secondary ions. A 90 μm × 90 μm area was analyzed with a 290 μm × 290 μm primary beam raster. Sputter depth profiling was completed with 1 keV cesium (Cs^+) beam.

Device characterization

The current density versus voltage (*J-V*) characteristics of the devices were tested under AM 1.5 G one-sun illumination (100 mW·cm^{-2}) and ambient air conditions without encapsulation. which was produced by an Enlitech SS-F5-3A solar simulator at room temperature. For the measurement of open-circuit voltage under different light intensities, the relationship between open-circuit voltage and light intensity could be described by the equation of $qV_{OC} = E_g + n_{ID}k_BTln\frac{I}{I_0}$, where q, k_B, T, I, E_g stand for electron charge, the Boltzmann constant, the absolute temperature, light intensity and optical bandgap of perovskite, respectively. The metal masks with an area of 0.1 cm^2 for single-junction devices and 1.0 cm^2 for tandem devices were employed to determine the active area. The incident photon to converted electron efficiency (IPCE) measurement was conducted to acquire the external quantum efficiency (EQE) spectra with a range from 300 to 1200 nm using g a QE measurement system (QE-R, EnliTech). The standard reference silicon cell and Ge to calibrate the light intensity. The *J-V* curves were recorded under continuous 1-sun illumination by Multi-channel Solar Cell Stability Testing system (Ezhou Zhongneng Optoelectronics Co., Ltd.) to evaluate the long-term stability of the devices. To isolate the intrinsic degradation of the perovskite active layer and its interfaces from external environmental factors, the long-term stability of tandem device was conducted in a N_2-flowed chamber. The chamber was placed in an air-conditioned room with an ambient temperature of 25-35°C. To mitigate

device self-heating under continuous illumination and bias, a small cooling fan was used externally to enhance air convection around the sample holder. A xenon lamp without ultraviolet filter was used as the light source. The MgF_2 layer is typically applied as an anti-reflection coating to improve optical coupling. In this study, we deliberately omitted such a layer to exclude its potential influence on the stability outcome. The electroluminescence (EL) spectra were conducted by a Keithley 2420 source meter and integrating sphere connected to a spectrophotometer (QE65Pro). The Electrochemical impedance spectroscopy (EIS) curves of the devices were obtained from CHI760E electrochemical workstation with a frequency of 0.1 Hz to 1MHz in a dark environment. The Mott-Schottky measurements were performed by a CHI760E electrochemical workstation (Shanghai Chenhua Instruments, Inc) at 8000 Hz with the applied voltages ranging from 1.2 to 0 V.

Calculation methods

For PL and TRPL measurements, the decay lifetime was fitted by the equation of $f(t) = A_1 exp^{-t/\tau_1} + A_2 exp^{-t/\tau_2} + B$ using biexponential decay model. B, A_1, and A_2 are constants associated with baseline offset and the contributions of fast (τ_1) and slow (τ_2) segments, respectively. The average carrier lifetime (τ_{ave}) can be determined from the formula of $\tau_{ave} = \frac{\sum A_i \tau_i^2}{\sum A_i \tau_i}$.

For *J-V* measurement, in the ohmic-like region, the current depends linearly on voltage. In the case of trap and doping-free semiconductors and non-limited charge carrier injection, the mobility can be inferred from this region using the equation of $J = 4\pi^2 \frac{\mu \kappa_B T}{q} \varepsilon_0 \varepsilon_r \frac{V}{L^3}$. Here, q is the elementary charge, μ is the mobility, k_BT is the thermal energy, ε_0 and ε_r are the vacuum and relative permittivity, respectively, and L is the layer thickness. If the semiconductor is (unintentionally) doped, the current can also

appear linear with voltage due to ohmic conduction. In this case, the analytical formula reads $J = q\mu N\frac{V}{L}$, where N is the carrier concentration.

The defect-state density (n_{trap}) of perovskite films can be calculated on the basis of the formula of $n_{trap} = \frac{2\varepsilon\varepsilon_0 V_{TFL}}{ed^2}$, where n_{trap} is the trap density, ε is the relative dielectric constant (24.4), ε_0 is the permittivity of vacuum (8.854×10^{-12} F m^{-1}), e is the element charge (1.602×10^{-19} C), and d is the thickness of perovskite absorber layer (530 nm).

For Mott-Schottky measurement, the formula of $\frac{1}{C^2} = \frac{2(V_{bi} - V)}{A^2 e\varepsilon\varepsilon_0 N}$ was used, where C is the capacitance of the space charge region, V_{bi} is built-in potential, V is the applied voltage, A is the area of devices, N is the carrier concentration. The V_{bi} value can be estimated from the intercept of Mott-Schottky curves with the x-axis.

For EL measurements, the voltage loss induced by the non-radiative recombination was evaluated from the formula of $\Delta V_{OC}^{nonrad} = -\frac{k_B T}{q}\ln\left(EQE_{EL}\right)$, where K_B, T, q, and EQE_{EL} are electron charge, Boltzmann constant, temperature and the electroluminescence efficiency, respectively.

For binding energy and the behavior of the electron localization function, calculations based on first-principles density functional theory (DFT) were conducted utilizing the Vienna Ab initio Simulation Package (VASP) in conjunction with the Projector Augmented Wave (PAW) methodology.[1, 2] The exchange-correlation functional was managed within the parameters of the Generalized Gradient Approximation (GGA), adopting the Perdew-Burke-Ernzerhof (PBE) functional.[3] We implemented a plane wave basis set with an energy cutoff set at 500 eV, and the geometric relaxation was carried through until the forces acting on each atom were less than 0.03 eV/Å. Brillouin zone sampling was carried out using a 1 × 1 × 1 k-point grid for all models. Electronic

self-consistency was converged to 1×10^{-5} eV. For the electron localization function (ELF) calculation process, the k-point setting was kept the same as in the geometry optimization. To further improve accuracy, the energy cutoff was increased to 600 eV and the electronic self-consistency criterion was tightened to 10^{-6} eV. Based on the framework of first-principles density functional theory calculations, the interface energy of a heterostructure can be evaluated using the following expression:

$$\gamma_{interface} = \frac{E_{interface} - E_{bulk,1} - E_{bulk,2}}{2A}$$

where $E_{\mathrm{interface}}$ is the total energy of the heterostructure system, $E_{bulk,1}$ and $E_{bulk,2}$ are the energies of the two bulk materials, A denotes the interfacial area.

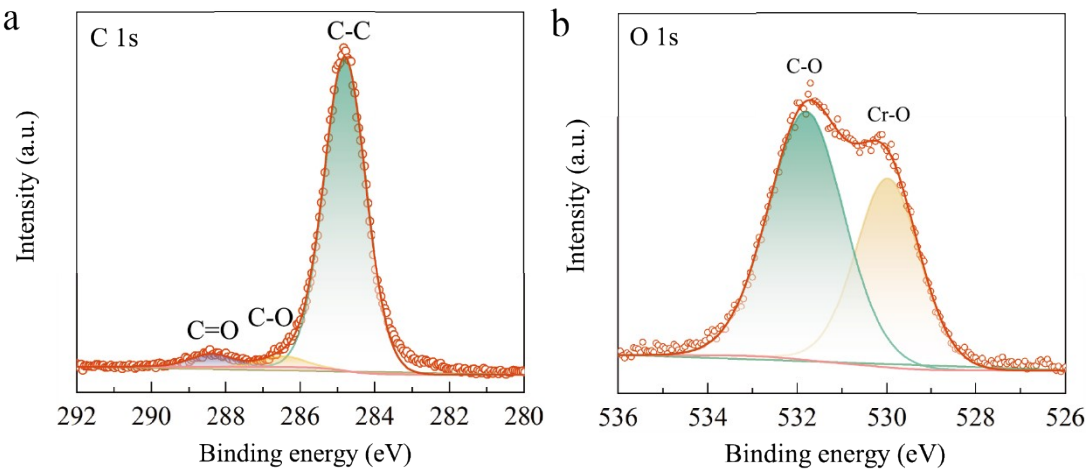

Figure S1. The XPS spectra of C 1s and O in CrO_X film.

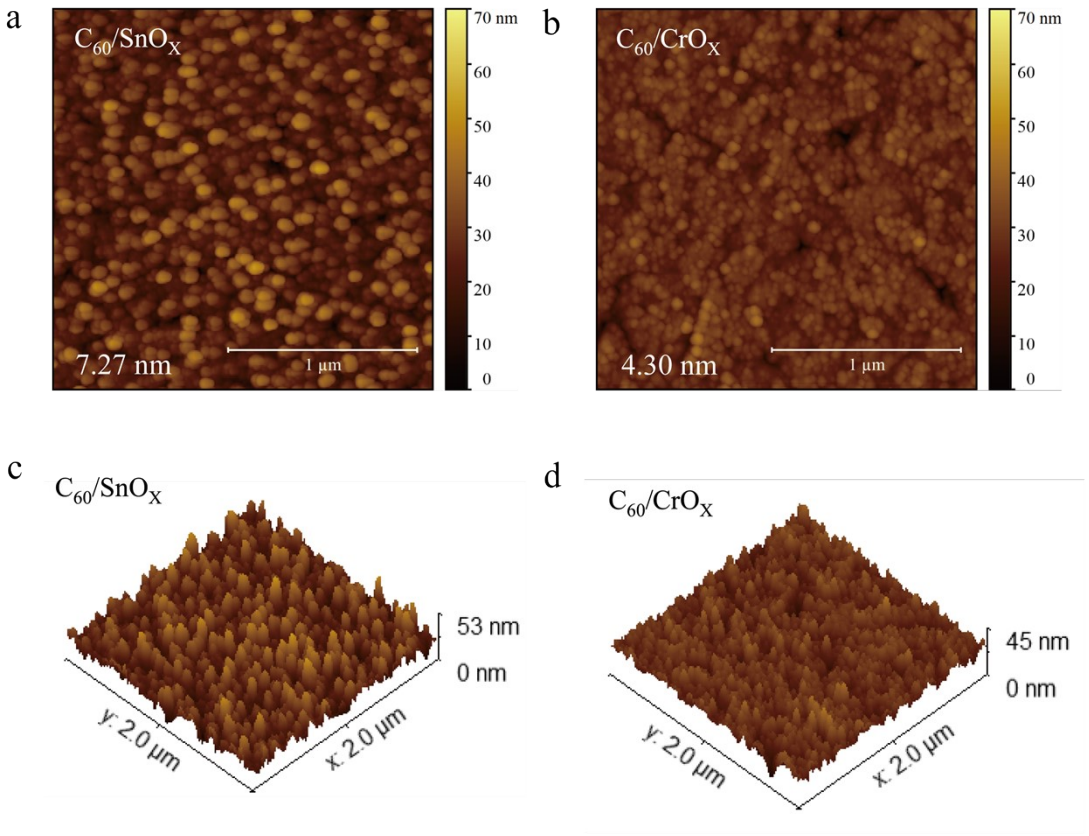

Figure S2. The roughness of C_{60}/SnO_X **a.** and C_{60}/CrO_X **b.** films. **c.** and **d.** The corresponding 3D AFM images.

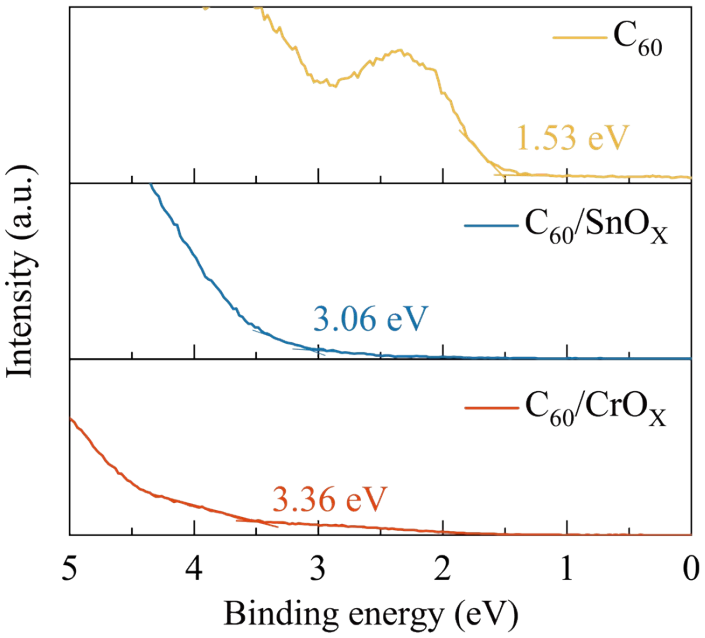

Figure S3. The UPS spectra of E_V-E_F of C_{60}, C_{60}/SnO_X and C_{60}/CrO_X films.

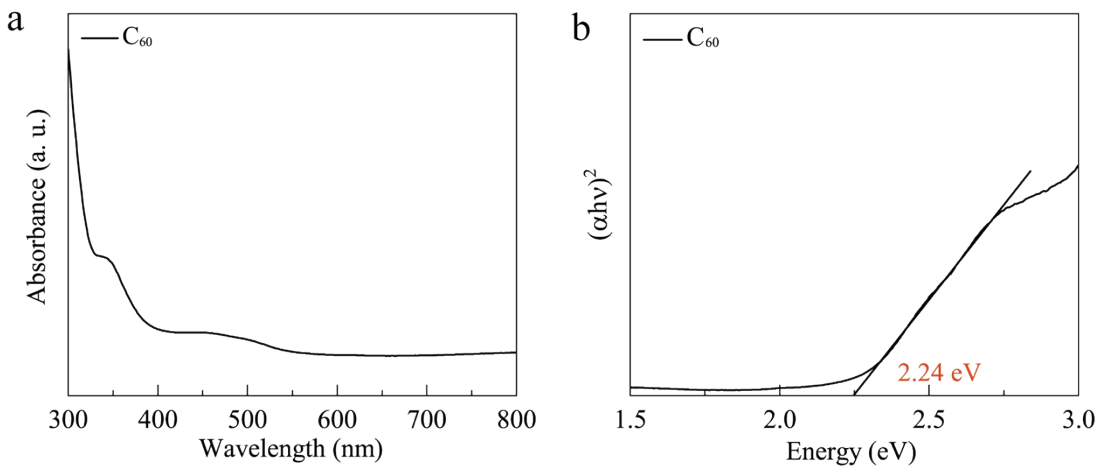

Figure S4. The ultraviolet-visible (UV-vis) absorption spectrum and Tauc plot of C_{60} film.

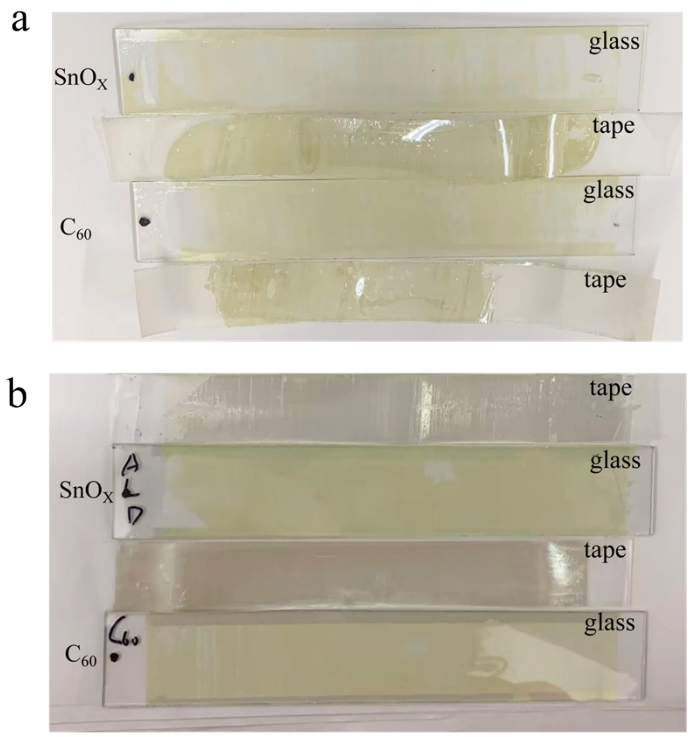

Figure S5. **a.** Picture of C_{60} and ALD SnO_X films after the tape peeling test. **b.** Picture of C_{60}/IZO and ALD SnO_X/IZO films after the tape peeling test.

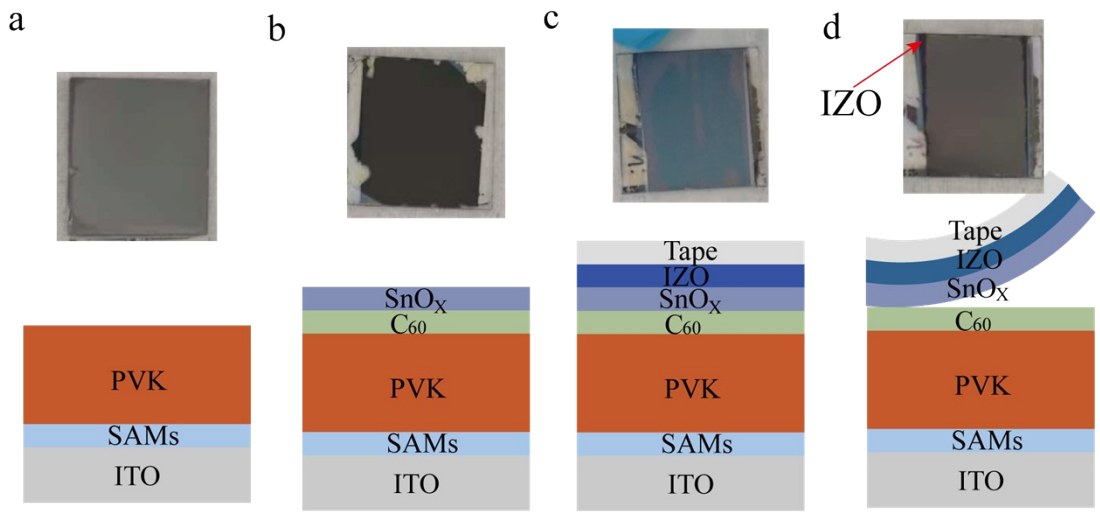

Figure S6. Picture of the perovskite films: **a.** pure perovskite film; **b.** PVK/C_{60}/SnO_X film; **c.** PVK/C_{60}/SnO_X/IZO film covered by tape; **d.** PVK/C_{60}/SnO_X/IZO film after peeling. Picture of the perovskite films: **a.** pure perovskite film; **b.** PVK/C_{60}/SnO_X film; **c.** PVK/C_{60}/SnO_X/IZO film covered by tape; **d.** PVK/C_{60}/SnO_X/IZO film after peeling.

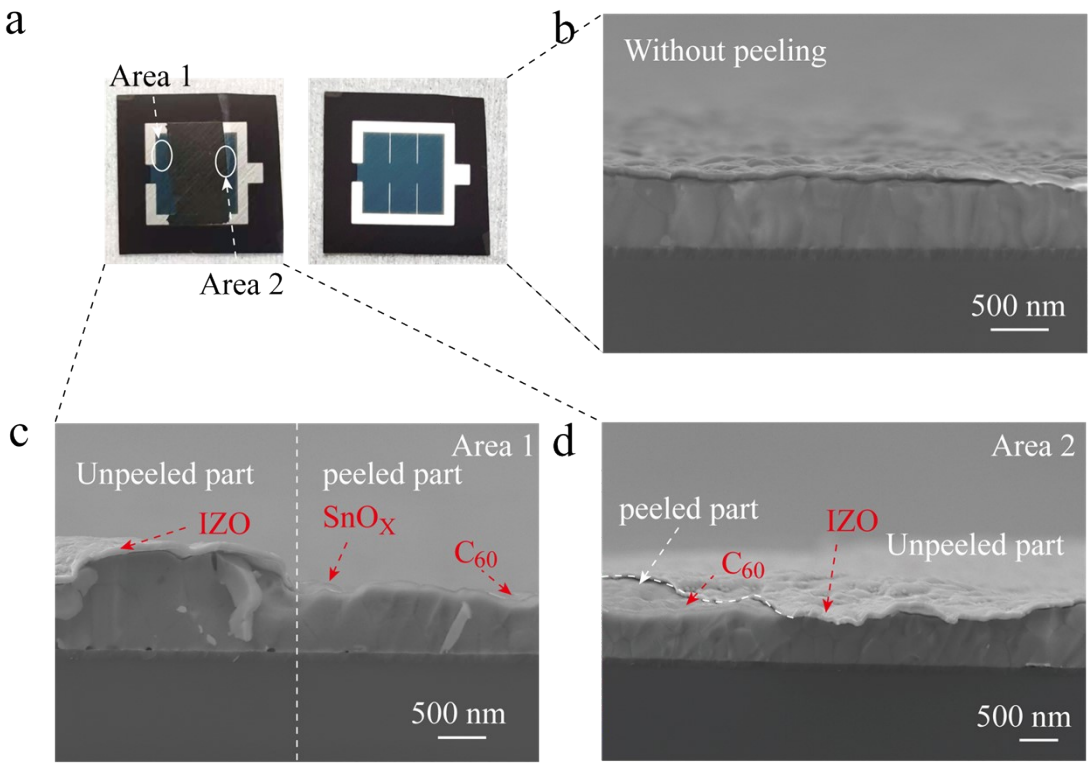

Figure S7. **a.** Picture of the pure tandem solar cell before and after the peeling. **b.** Cross-sectional SEM images of tandem device. **c.** and **d.** Cross-sectional SEM images of peeled tandem at the interface between the peeled and unpeeled parts, which is marked by white cycle in **a**.

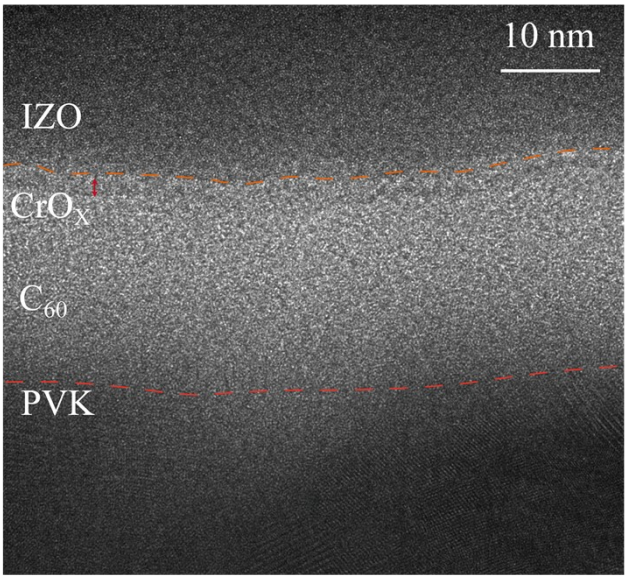

Figure S8. High high-resolution STEM images of CrO_X-based device.

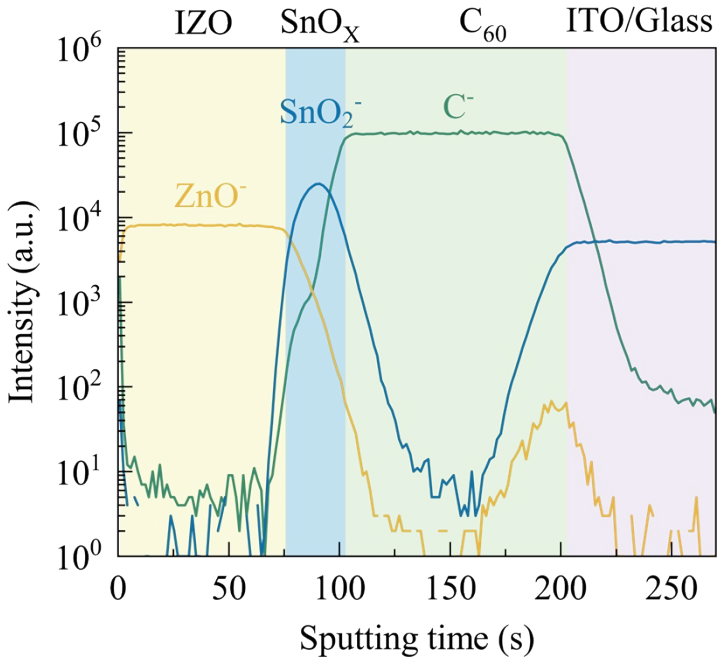

Figure S9. ToF-SIMS in-depth profiles (negative ions) of ITO/C_{60}/SnO_X film.

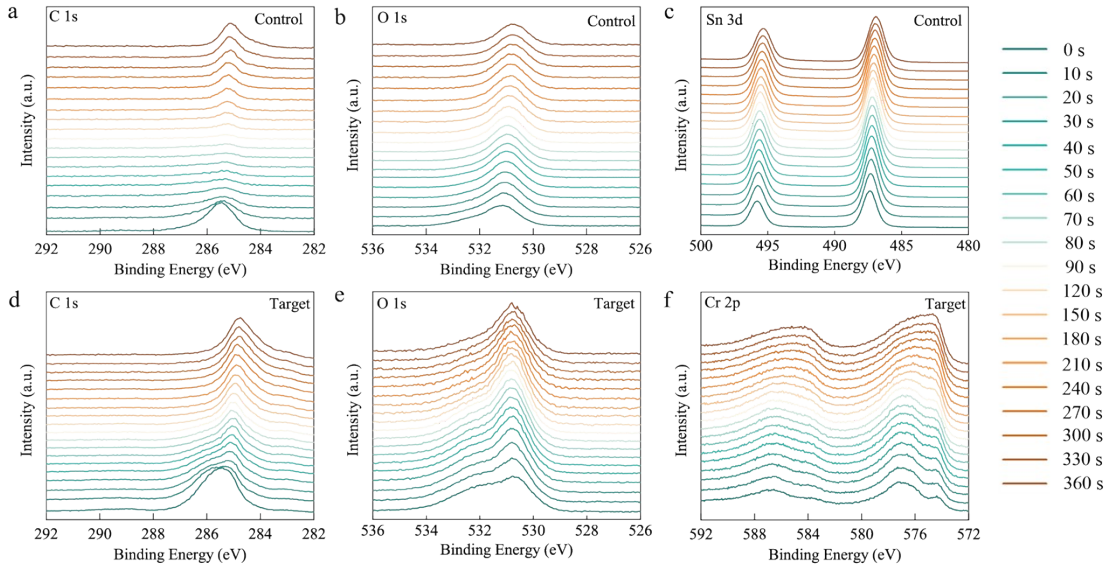

Figure S10. The etching XPS spectra of C 1s, O 1s, Sn 3d and Cr 2p for C_{60}/SnO_X and C_{60}/CrO_X films.

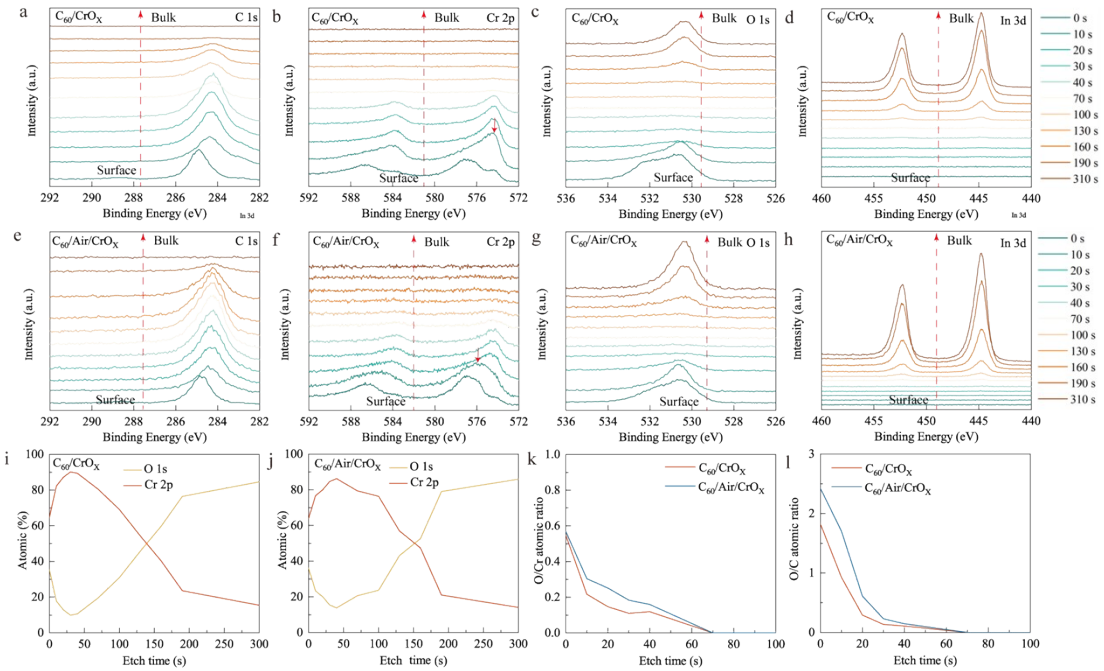

Figure S11. a-h. The etching XPS spectra of C 1s, O 1s, In 3d and Cr 2p for C_{60}/CrO_X and $C_{60}/Air/CrO_X$ films. Depth profile XPS results of O and Cr in C_{60}/CrO_X **i.** and $C_{60}/Air/CrO_X$ **j.** films. The corresponding O/Cr **k.** and O/C **l.** atomic ratios.

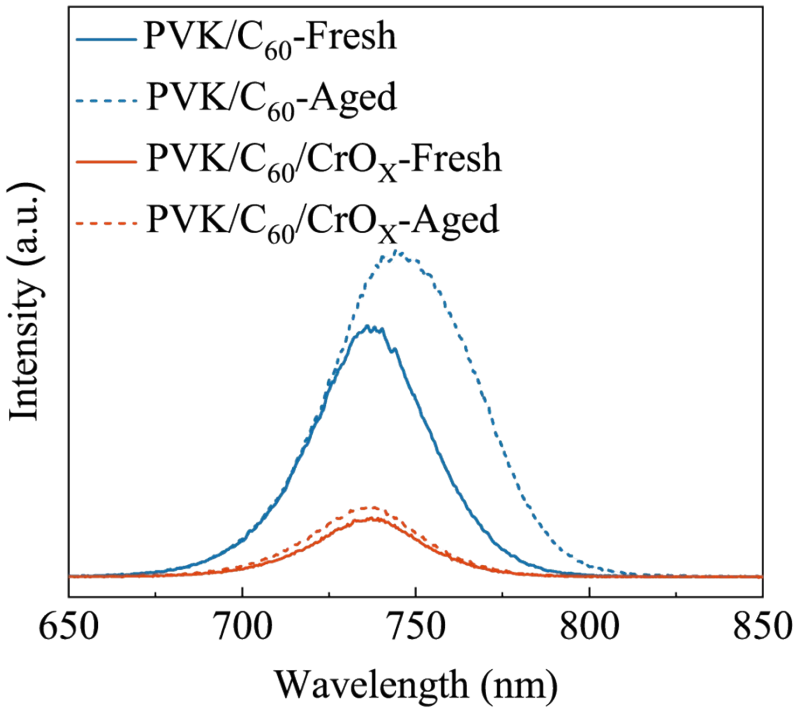

Figure S12. The fresh and aged PL patterns of PVK/C_{60} and PVK/C_{60}/CrO_X films.

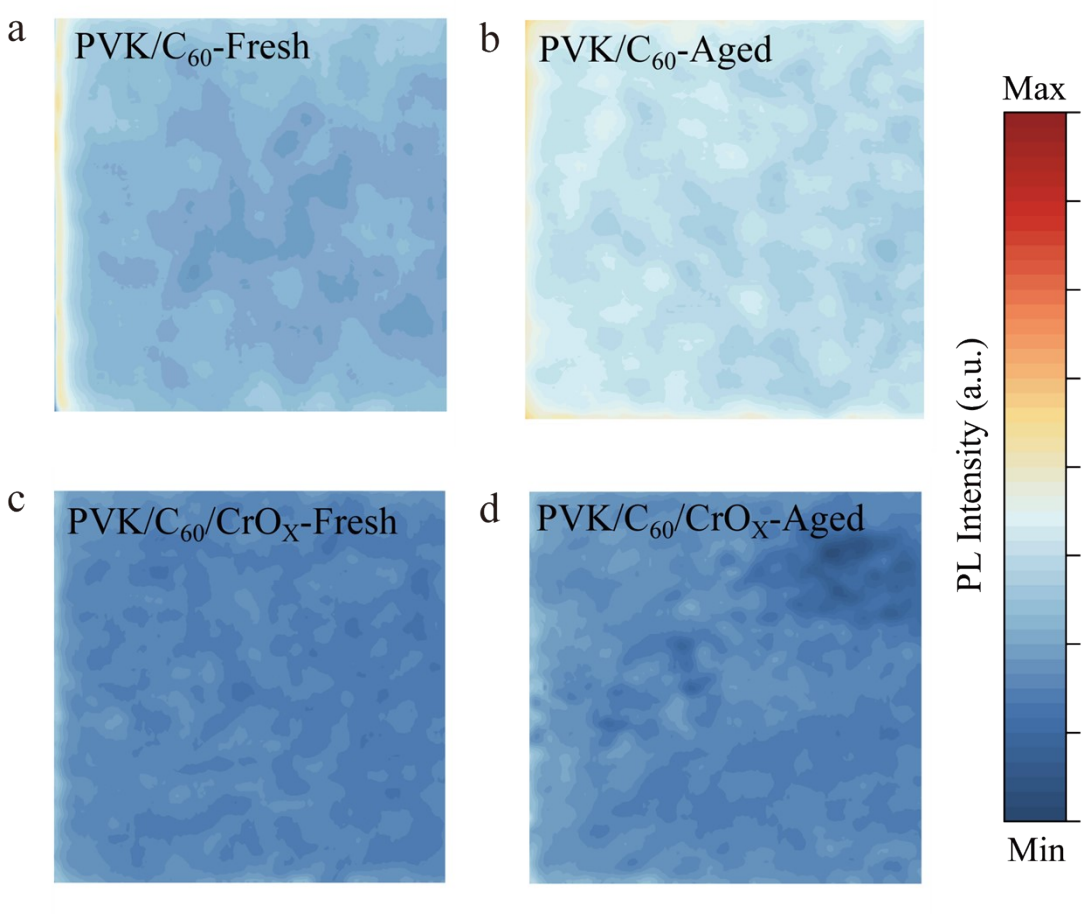

Figure S13. The fresh and aged PL mapping of PVK/C_{60} and $PVK/C_{60}/CrO_X$ films.

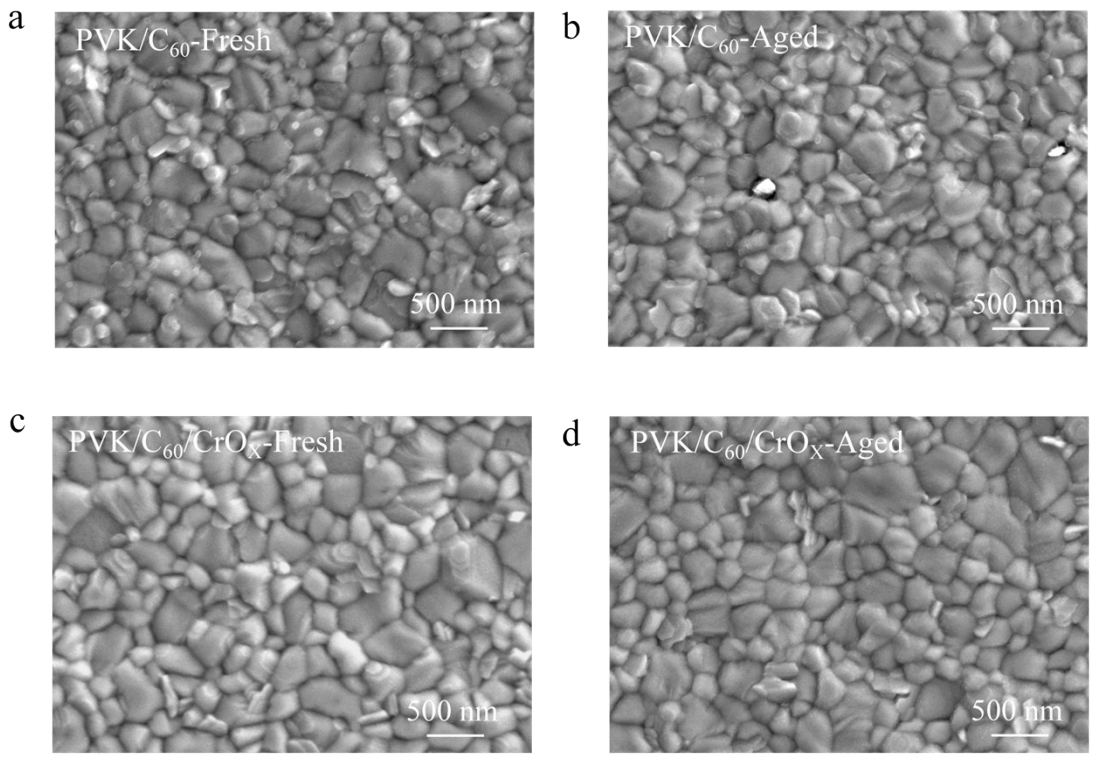

Figure S14. SEM images of PVK/C_{60} and $PVK/C_{60}/CrO_X$ films before and after 6-hour aging in ambient air.

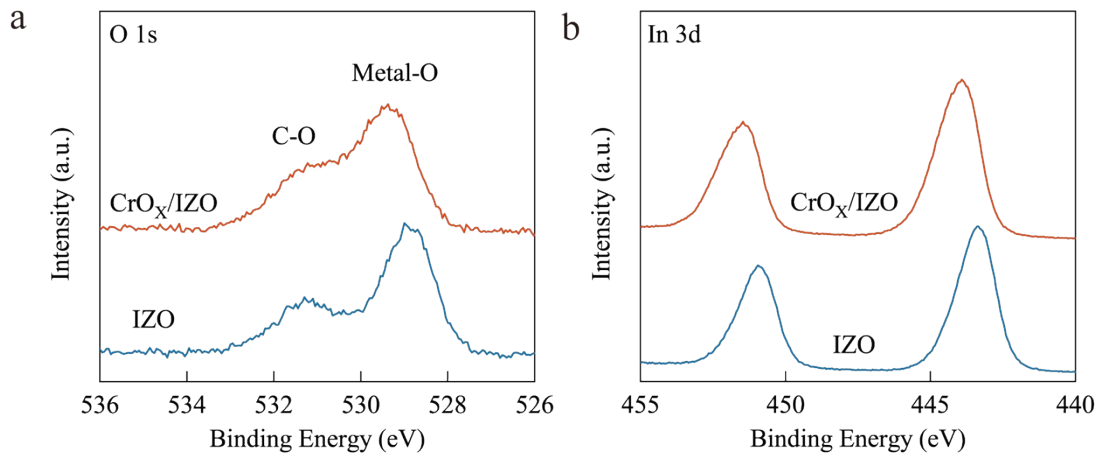

Figure S15. The XPS spectra of O 1s **a.** and In 3d **b.** in IZO and CrO_X/IZO films.

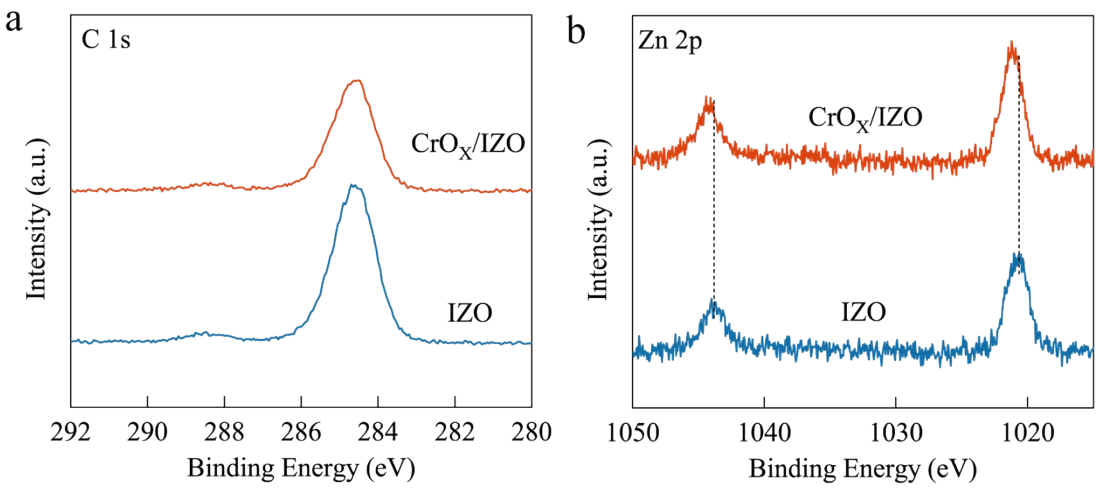

Figure S16. The XPS spectra of C 1s and Zn 2p.

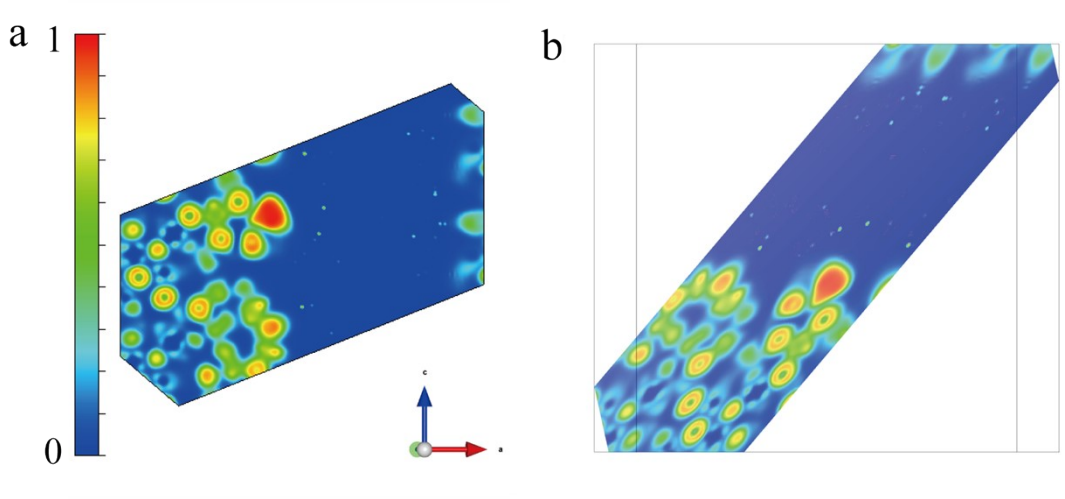

Figure S17. a. 2D ELF plot containing the chemical bond between Cr-O and In-O. **b.** The corresponding 3D ELF plot.

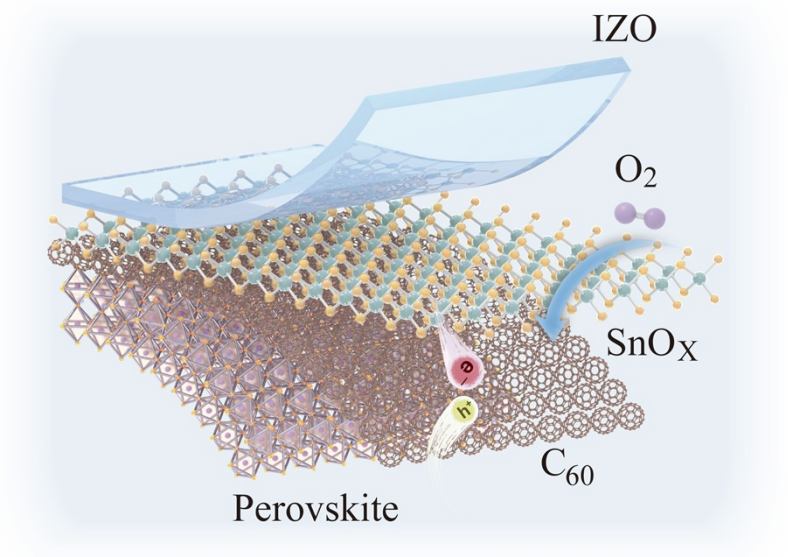

Figure S18. Schematic illustration of SnO_X-based device.

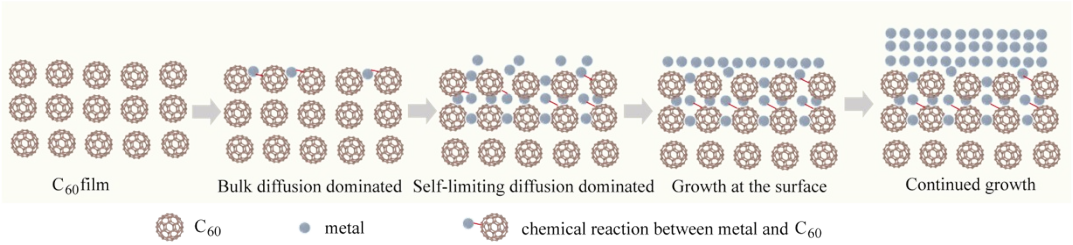

Figure S19. The diffusion mechanism of Cr metal on the C_{60} layer.

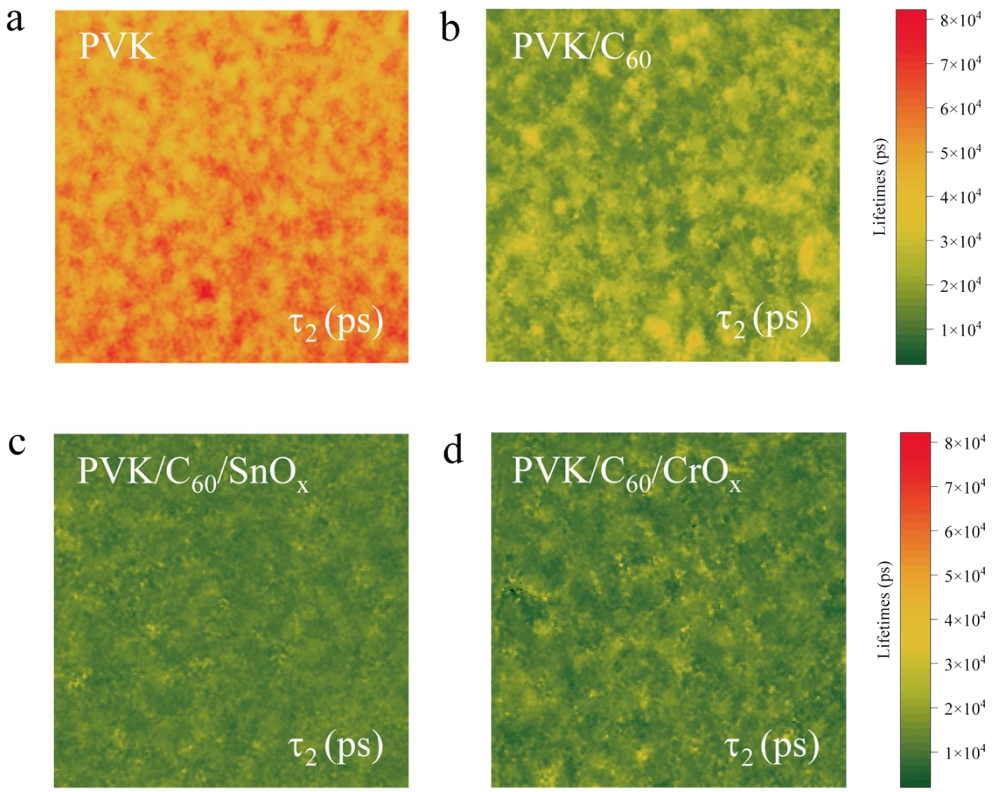

Figure S20. a-d. FLIM mapping images of PVK, PVK/C_{60}, PVK/C_{60}/SnO_X and PVK/C_{60}/CrO_X films, respectively, which indicates the lifetime of τ_2.

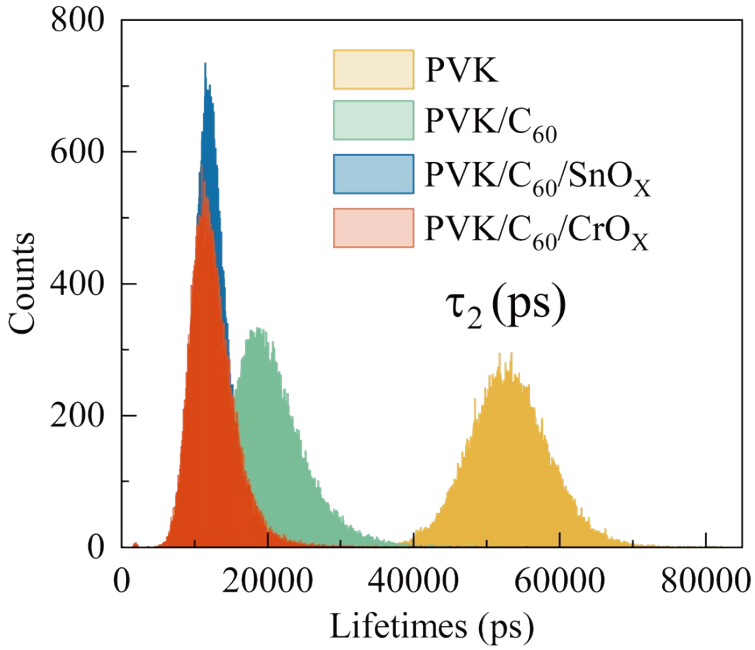

Figure S21. The statistic distribution of lifetime τ_2 extracted from the lifetime mapping.

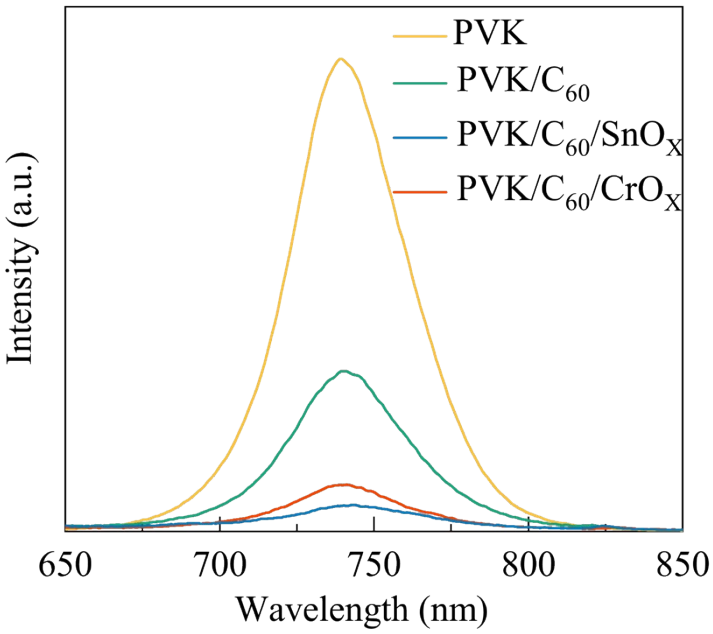

Figure S22. The PL patterns of PVK, PVK/C_{60}, PVK/C_{60}/SnO_X and PVK/C_{60}/CrO_X films.

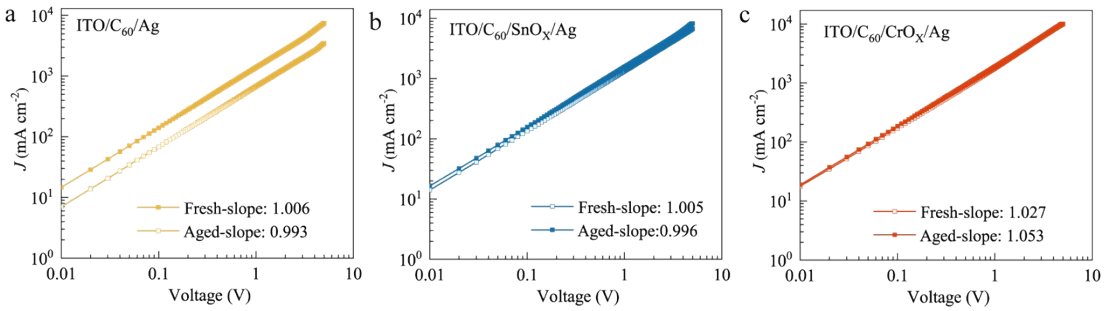

Figure S23. The *J-V* characteristics of electron-only devices with the configuration of **a.** ITO/C_{60}/Ag, **b.** ITO/C_{60}/SnO_X/Ag and **c.** ITO/C_{60}/CrO_X/Ag. For aged devices, these films were aged at ambient condition for 24 h before deposition of Ag (25-35ºC, 60%-80% RH).

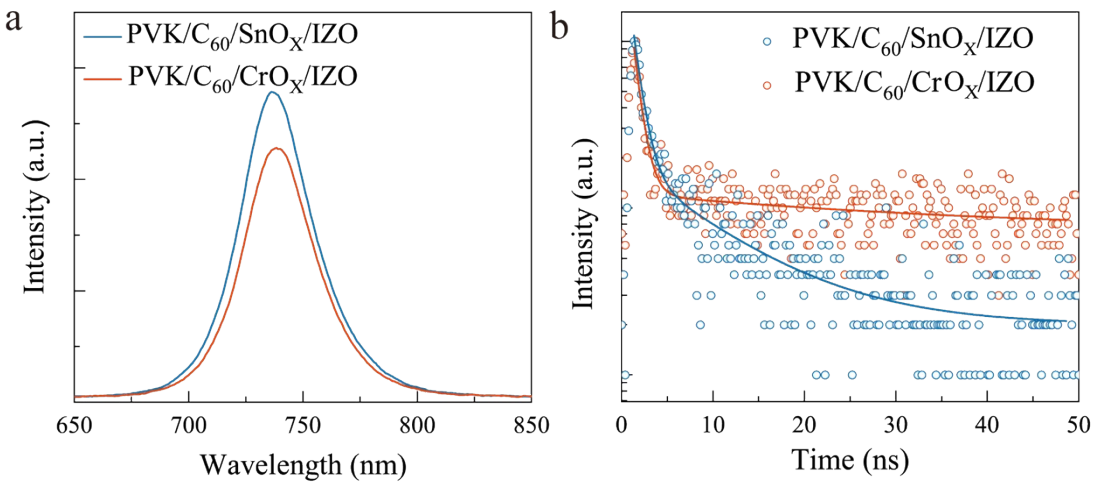

Figure S24. PL **a.** and TRPL **b.** spectra of PVK/C_{60}/SnO_X/IZO and PVK/C_{60}/CrO_X/IZO films.

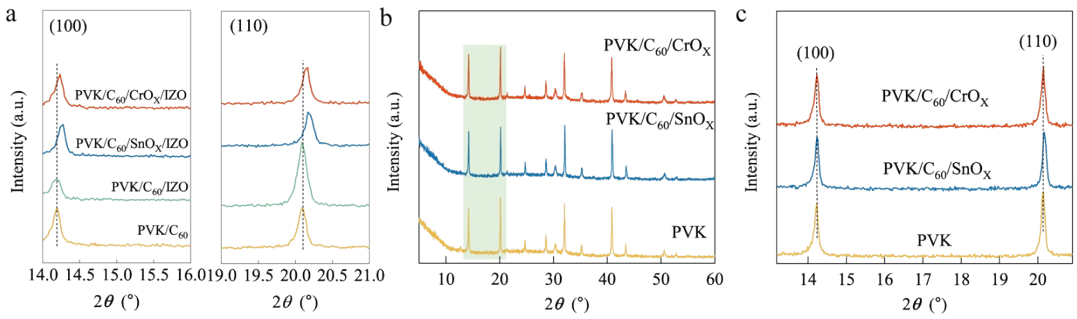

Figure S25. a. The amplified XRD patterns of PVK/C_{60}, $PVK/C_{60}/IZO$, $PVK/C_{60}/SnO_X/IZO$ and $PVK/C_{60}/CrO_X/IZO$. **b.** The XRD patterns of perovskite films without IZO. **c.** The amplified XRD patterns of the green region in **c**.

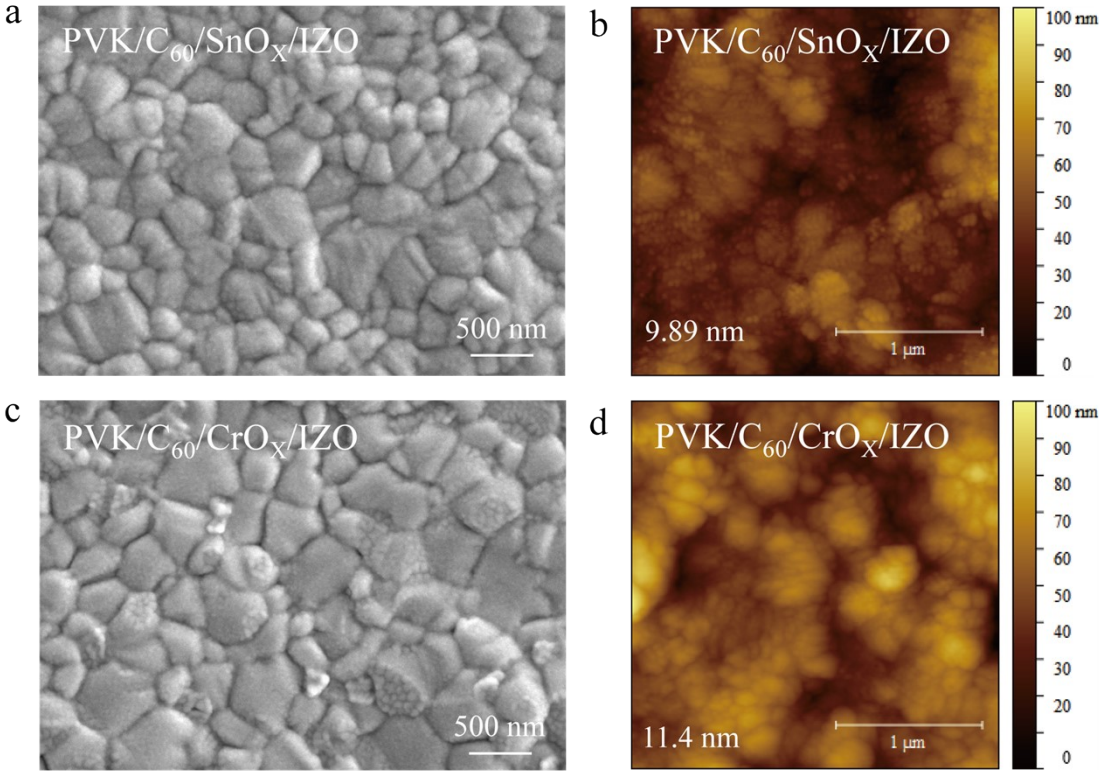

Figure S26. The SEM and AFM images of perovskite films with IZO based on SnO_X and CrO_X buffer layer.

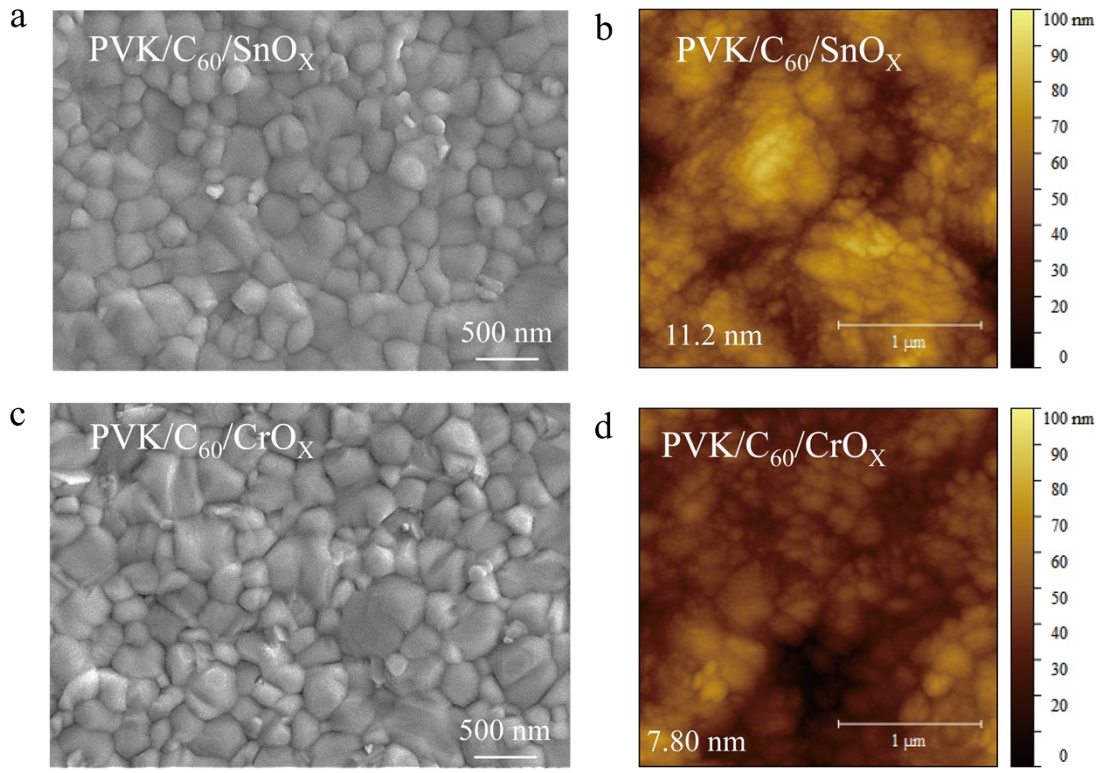

Figure S27. The SEM and AFM images of perovskite films without deposing IZO based on SnO_X and CrO_X buffer layer.

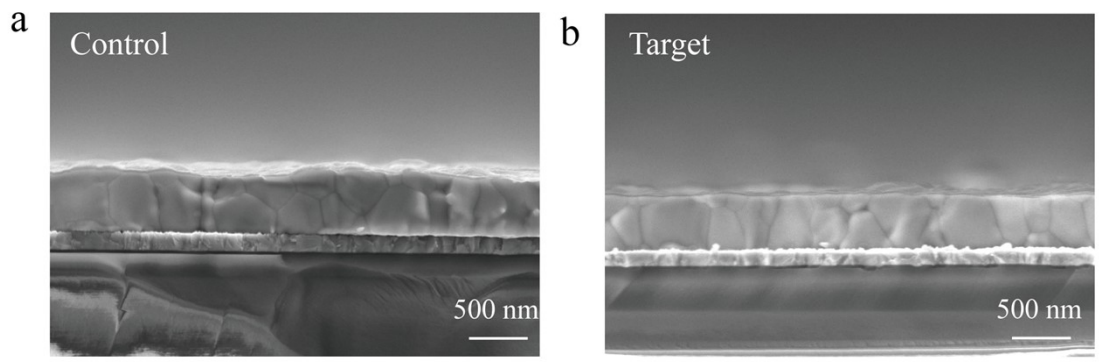

Figure S28. The cross-sectional SEM images of control and target devices.

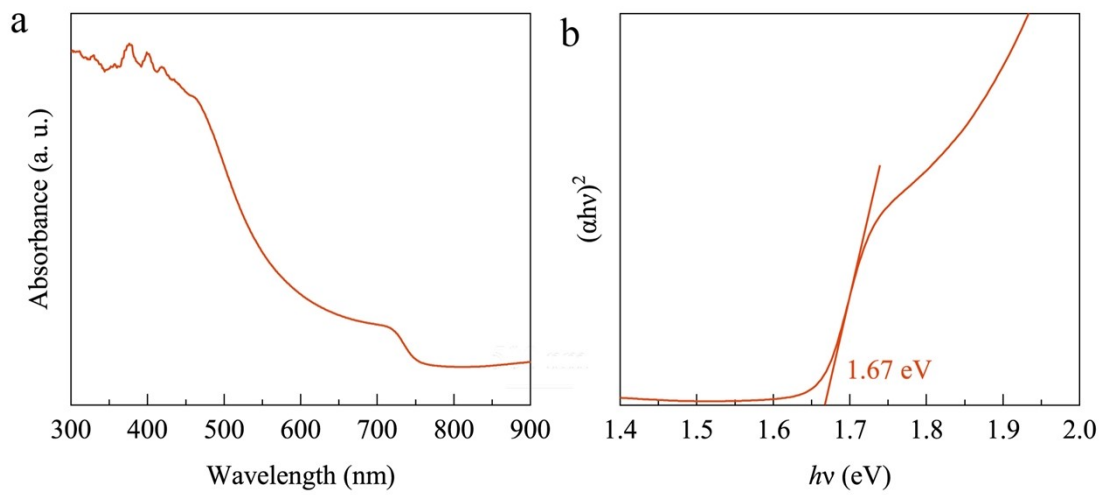

Figure S29. The ultraviolet-visible (UV-vis) absorption spectrum and Tauc plot of perovskite film.

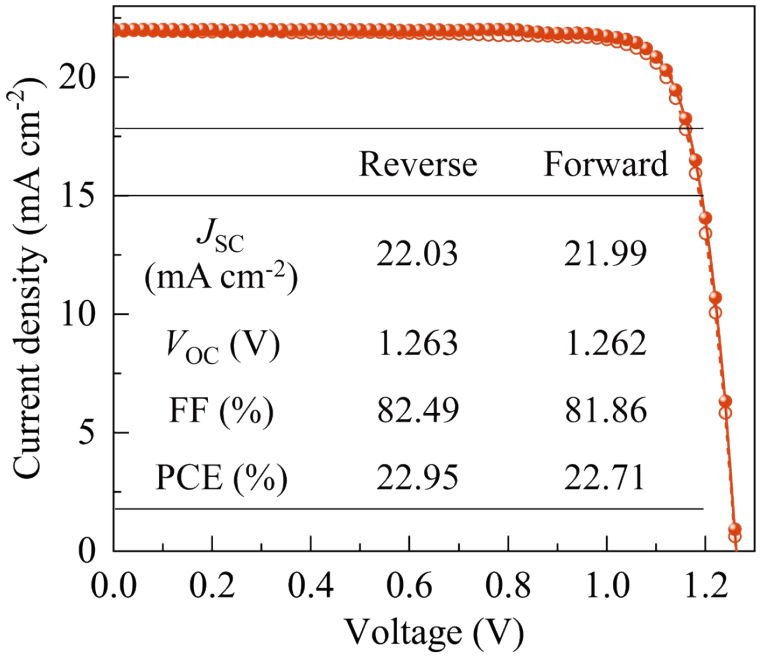

Figure S30. The *J-V* curves of the champion target device with the highest V_{OC} under simulated AM1.5G solar illumination.

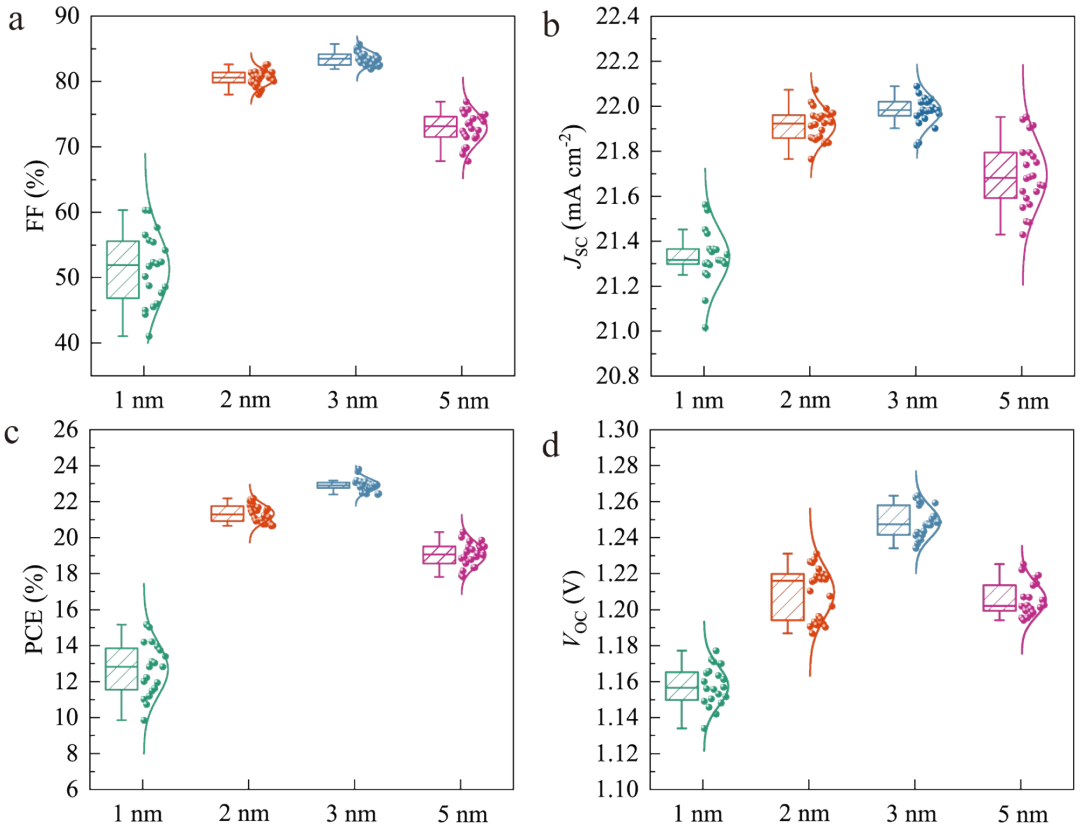

Figure S31. Statistical distribution of FF, J_{SC}, PCE and V_{OC} of the device based on the different thicknesses of CrO_X film.

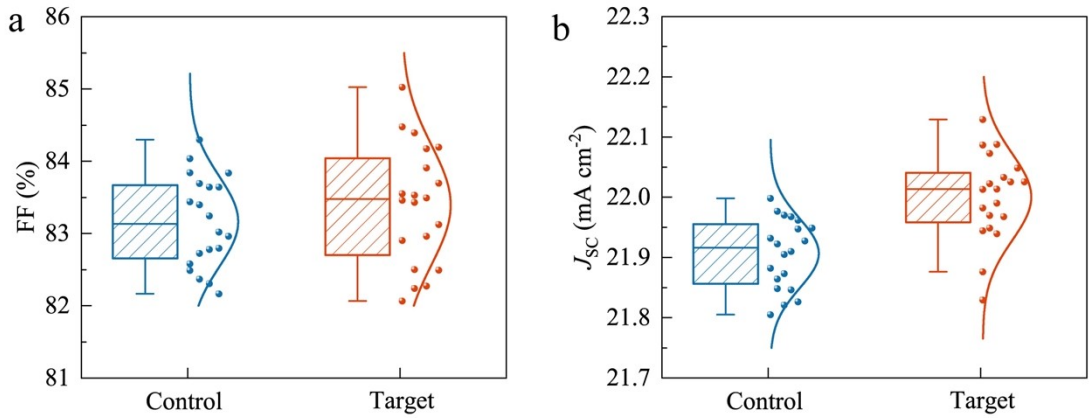

Figure S32. Statistical distribution of FF and J_{SC}.

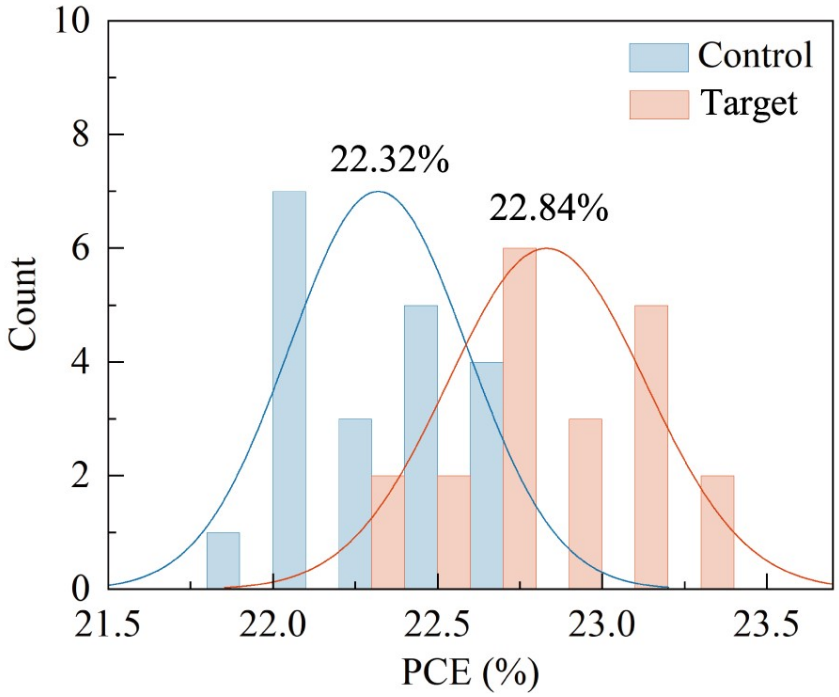

Figure S33. The PCE distribution of approximately 20 devices.

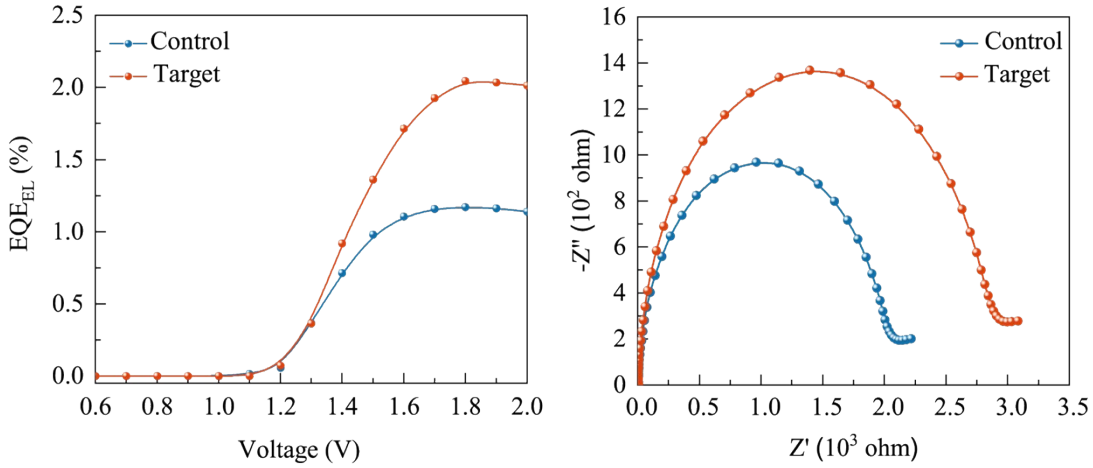

Figure S34. EQE_{EL} spectra **a.** and Nyquist plots measured in the dark at a bias voltage of 1.0 V **b.** of control and target devices.

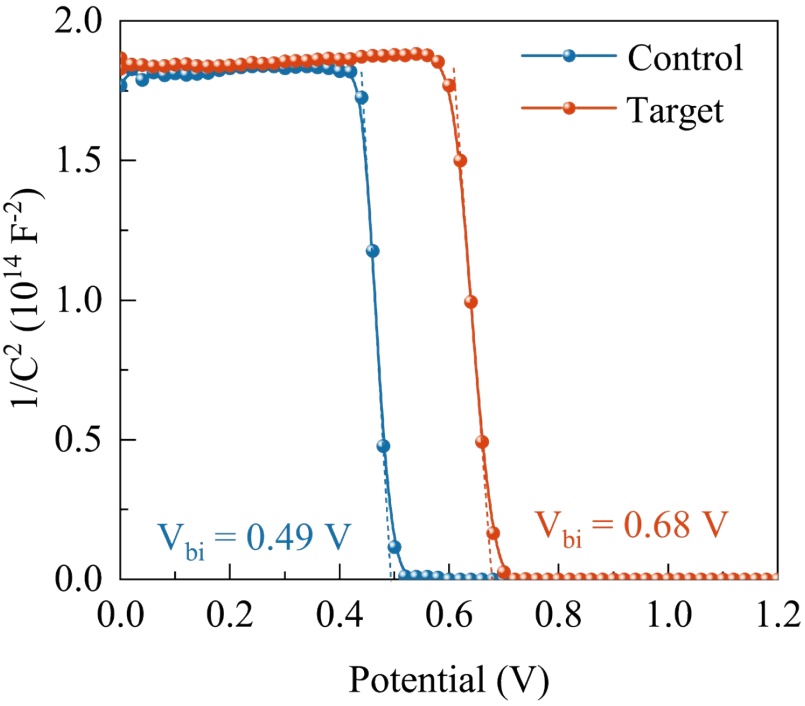

Figure S35. The Mott-Schottky curves of control and target device.

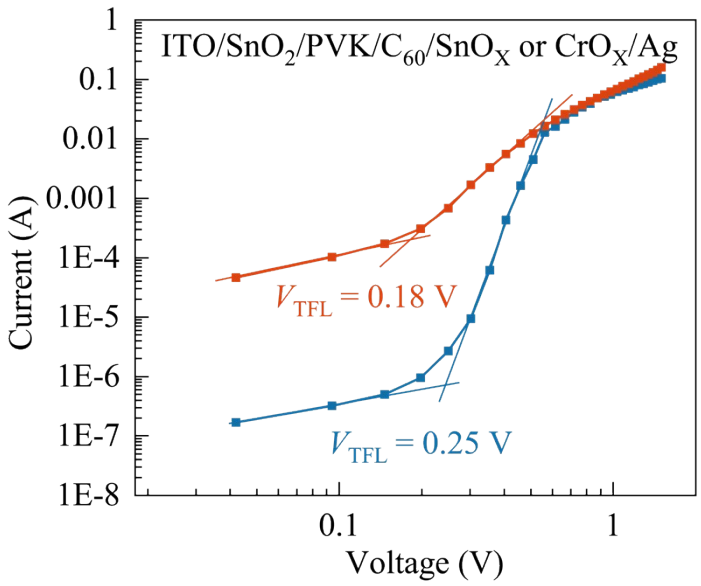

Figure S36. The SCLC curves of electron-only devices based on SnO_X and CrO_X buffer layer.

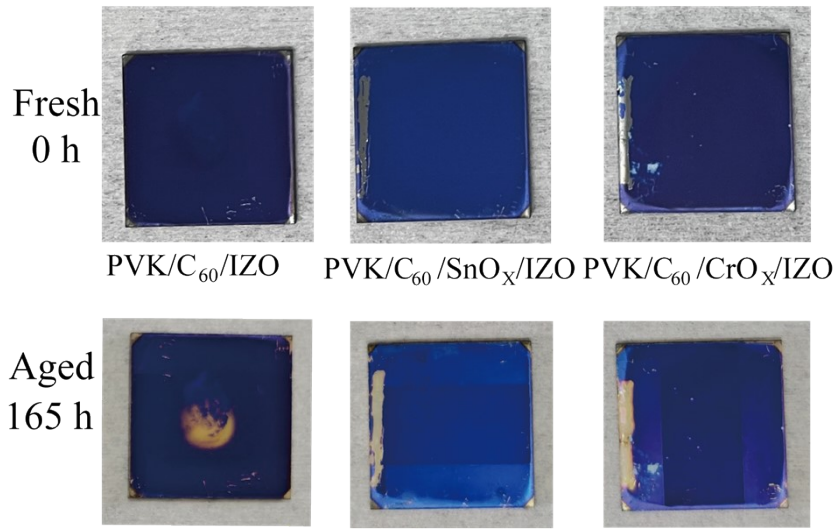

Figure S37. Photographs of perovskite films under the ambient air with relative humidity of 60-80%.

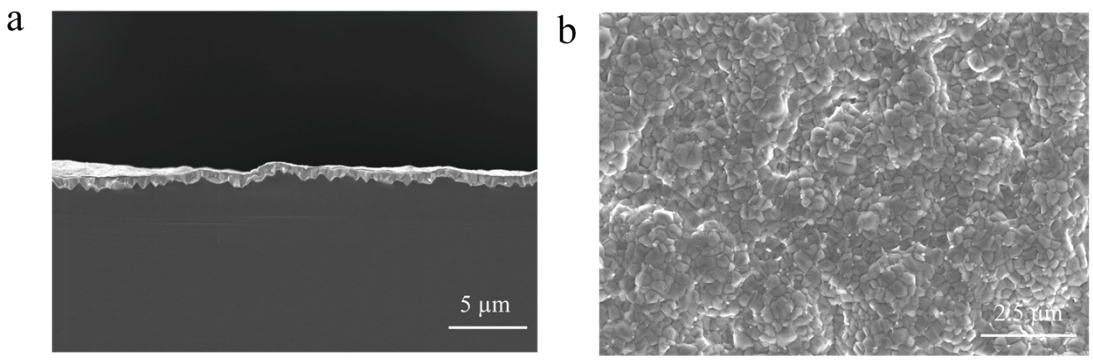

Figure S38. The cross-sectional and top-view SEM images of the perovskite top cell deposited on the double-side textured silicon bottom cell.

No: NBMTEC-SC-250707-0070

中国认可
国际互认
检测
TESTING
CNAS L16821

New Materials Testing and Evaluation Platform

Zhejiang Regional Center

Ningbo New Materials Testing and Evaluation Center

TEST REPORT

Entrusting Party	Ningbo Institute of Materials Technology & Engineering, CAS
Address of Entrusting Party	No. 1219, Zhongguan West Road, Zhenhai District, Ningbo City, Zhejiang Province, P. R. China
Sample Name	Perovskite / TOPCon tandem solar cells
Test Date	7th July, 2025

宁波新材料测试评价中心有限公司 检验检测专用章

COMPILED BY	黄腾祚
REVIEWED BY	
APPROVED BY	
APPROVED DATE	2025. 07. 16

Address: Room 1-2, No.21, building 2, East District, New material innovation center, Ningbo National Hi- Tech Zone, Ningbo. Tel: 0574-87528296 Post code: 315201

Sample Information

Sample Name	Perovskite / TOPCon tandem solar cells
Serial No.	250707-SC0070
Measurement Item	I-V characteristic; Area; Spectral response (SR)
Measurement Environment	24.9 ± 2.0 °C; 53.8% ± 5% R.H
Measurement Address	No.1819, Yongmao East Road, Zhenhai District, Ningbo, Zhejiang

Measurement of I-V characteristic

Reference Cell	RQN211400
Reference Cell Type	Mono-Si, Quartz glass
Calibration Value/Date	132.7 mA/ May. 2025
Measurement Conditions	Standard test condition (STC): Spectral distribution: AM 1.5G according to IEC 60904-3:2019 Ed.3; Irradiance: 1000 ± 50 W/m^2; Temperature: 25.0 ± 2.0°C.
Measurement Equipment	AAA Steady dual light source solar simulator (WXS-90S-L2); Measuring Microscope (Mitutoyo MFA3017D); SR measurement system (BUNKOUKEIKI CEP-25ML).
Measurement Method	Area measurement: Based on the SJ/T 11630-2016; SR measurement: Based on the IEC 60904-8-1: 2017; I-V measurement: Logarithmic sweep in both direction (I_{SC} to V_{OC}, V_{OC} to I_{SC}) during one flash based on IEC 60904-1-1: 2017; Steady-State measurement: ☑ Maximum power point tracking (MPPT): 300 seconds by Perturb & Observe method. ☐ Asymptotic Pmax scan.

Spectral Mismatch Factor	Spectral Mismatch Factor (SMM) of the Top Cell=1.008; SMM of the Bottom Cell=1.003; SMM was calculated according to IEC 60904-7:2019 and I-V correction according to IEC60891:2021.
Measurement Uncertainty	Area[da]: 0.18% (k=2); I_{SC}: 1.6% (k=2); V_{OC}: 1.2% (k=2); P_{max}: 2.1% (k=2); Eff: 2.48% (k=2)
Notes	■ Fast I-V scans are marked with "Unofficial Measurement" label because the results for unstable devices may be unreliable at high voltage bias rates. ■ The results apply only at the time of the test, and do not imply future performance. ■ The uncertainty stated is the expanded uncertainty resulting from multiplying the standard uncertainty by the coverage factor k=2, with a probability of 95% within the assigned interval.

------Measurement Results------

1. Area Measurement Data

	Area[da]
Test 1	0.965 cm^2
Test 2	0.966 cm^2
Test 3	0.966 cm^2
Average	0.966 cm^2

■ Designated illumination area defined by a thin metal mask was measured by a measuring microscope.

2. Fast I-V Scan Measurement Data and I-V Curves under STC

Forward Scan (I_{SC} to V_{OC})	
I_{SC}	20.142 mA
V_{OC}	1.9346 V
Pmax	31.144 mW
Ipm	18.772 mA
Vpm	1.6591 V
FF	79.92%
Eff	32.24%

Unofficial Measurement

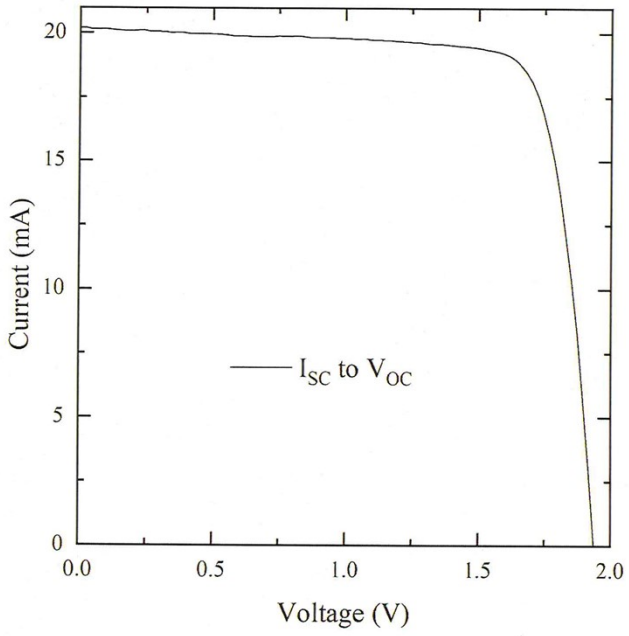

NOT A STABILIZED, REPORTABLE MEASUREMENT

Statement: 1. The test result presented in this report relate only to the object tested,
2. This test report may not be copied or partially intercepted without the written approval of the laboratory,
3. Any dissidence should be demurred within 15 days.

Reverse Scan (V_{OC} to I_{SC})	
I_{SC}	20.148 mA
V_{OC}	1.9354 V
Pmax	31.413 mW
Ipm	18.990 mA
Vpm	1.6541 V
FF	80.55%
Eff	32.51%

Unofficial Measurement

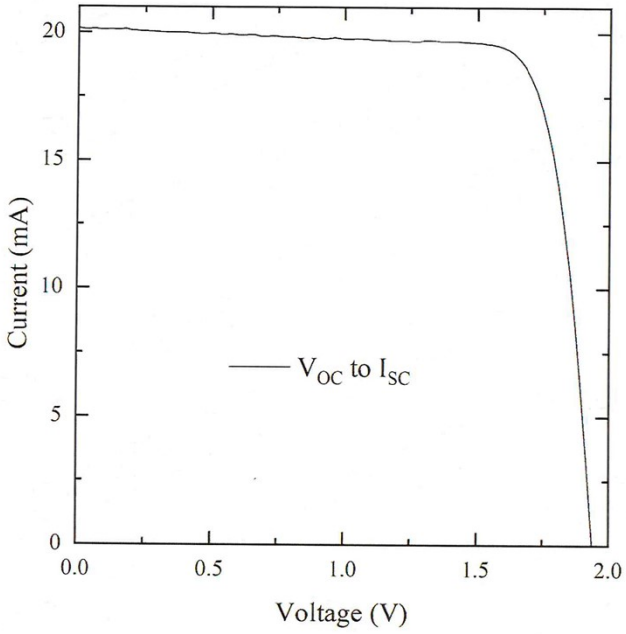

NOT A STABILIZED, REPORTABLE MEASUREMENT

Statement: 1. The test result presented in this report relate only to the object tested,
2. This test report may not be copied or partially intercepted without the written approval of the laboratory,
3. Any dissidence should be demurred within 15 days.

No: NBMTEC-SC-250707-0070

3. Steady-State Measurement (Method: MPPT) Data and Curves under STC

Maximum Power Point Tracking	
Pmax	31.412 mW
Ipm	18.882 mA
Vpm	1.6636 V
Eff	32.51%

■ Measurement data for steady-state measurement (MPPT) under STC in the table was the mean value acquired during the final 30 seconds of the 300-second test.

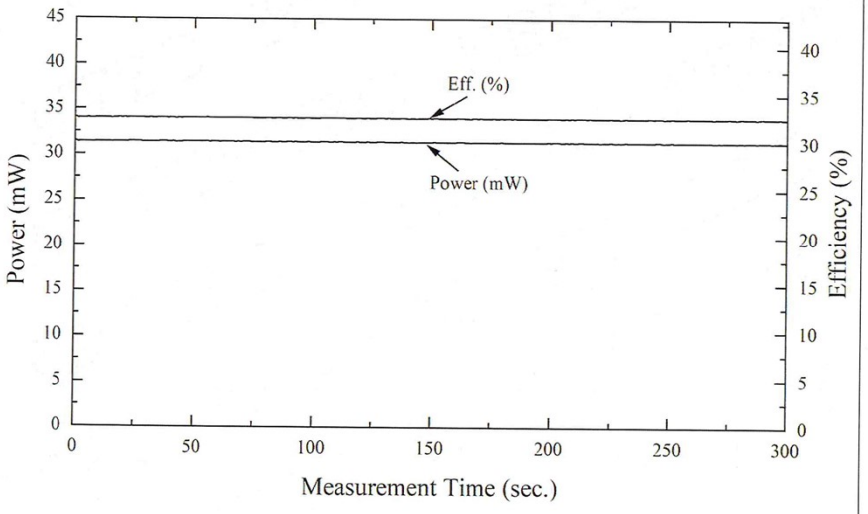

-----End of Report-----

Remarks:

1. This report is solely intended for the exclusive use of the client, and the data and results contained within are strictly for purposes of scientific research, educational instruction, internal quality assurance within the enterprise, and product innovation and development.
2. Sample information is provided by the clients, and the company is not responsible for its authenticity.

Statement: 1. The test result presented in this report relate only to the object tested,
2. This test report may not be copied or partially intercepted without the written approval of the laboratory,
3. Any dissidence should be demurred within 15 days.

5 / 5

Figure S39. The certificated report of one our champion tandem devices at Zhejiang Regional Center.

Table S1. The carrier lifetime of PVK, PVK/C_{60}, PVK/C_{60}/SnO_X and PVK/C_{60}/CrO_X films, which is determined from FLIM mapping using biexponential model fitting.

	PVK	PVK/C_{60}	PVK/C_{60}/SnO_X	PVK/C_{60}/Cr
τ_1 (ns)	5.54	2.43	2.34	1.48
τ_2 (ns)	53.08	20.34	12.61	12.49
A_1	88.83%	94.88%	94.31%	98.14%
A_2	11.17%	5.12%	5.69%	1.86%
τ_{ave} (ns)	31.51	8.00	4.86	2.99

Table S2. Summary of the state-of-the-art performances of wide-bandgap *p*-i-*n* devices (around 1.68 eV) reported in the literature.

Buffer layer	V_{OC} (V)	J_{SC} (mA cm^{-2})	FF (%)	PCE (%)	E_g (eV)	Year	Ref.
SnO_2	1.19	20.9	81.6	20.3	1.68	2023	[4]
BCP	1.239	21.16	82.50	21.63	1.68	2023	[5]
BCP	1.242	20.41	82.97	21.02	1.68	2023	[6]
SnO_2	1.28	-	-	21.5	1.68	2023	[7]
SnO_2	1.262	20.9	82.7	21.8	1.67	2023	[8]
BCP	1.25	21.5	84.5	22.7	1.68	2023	[9]
BCP	1.24	21.7	85.5	23.1	1.67	2023	[10]
SnO_2	1.246	21.49	86.53	23.18	1.67	2024	[11]
SnO_2	1.25	21.05	84.34	22.06	1.67	2024	[12]
BCP	1.22	21.48	82.88	21.72	1.68	2024	[13]
BCP	1.26	19.5	84.0	20.6	1.67	2024	[14]
SnO_2	1.275	21.68	84.83	23.45	1.68	2024	[15]
BCP/In_2O_3	1.23	19.73	83.00	20.20	1.68	2024	[16]
Sn-In_2O_3	1.21	20.47	82.02	20.34	1.68	2024	[17]
BCP	1.265	21.74	84.10	23.13	1.68	2025	[18]
BCP	1.270	21.95	82.17	22.88	1.68	2025	[19]
SnO_2	1.286	21.123	83.894	22.795	1.68	2025	[20]
SnO_2	1.30	22.4	80.2	23.4	1.68	2025	[21]

SnO_2	1.260	21.82	85.15	23.41	1.68	2025	[22]
BCP	1.254	20.77	85.6	22.3	1.68	2025	[23]
BCP	1.26	21.50	85	23.33	1.67	2025	[24]
MgO_X	1.22	20.65	84.66	21.33	1.68	2025	[25]
RPD-ITO	1.242	21.26	82.57	21.33	1.67	2025	[26]
CrO_X	1.251	22.01	84.48	23.27	1.67	2025	This work

Table S3. Summary of the state-of-the-art performances of monolithic perovskite/silicon tandems based on the TOPCon reported in the literature.

V_{OC} (V)	J_{SC} (mA cm^{-2})	FF (%)	PCE (%)	Cer. PCE	Area (cm^2)	Year	Ref.
1.74	19.5	74.7	25.1	-	1.42	2019	[27]
1.80	19.2	81.8	28.5	28.2	0.124	2022	[28]
1.73	18.78	80.31	26.06	25.84	0.1387	2022	[29]
1.799	19.4	81.64	28.49%	-	0.124	2022	[30]
1.76	17.8	74	23.81	-	1.0	2023	[31]
1.78	18.8	81.8	27.4	26.3	0.9491	2023	[32]
1.85	19.4	81.8	29.3	29.0	0.132	2023	[33]
1.688	16.1	69.3	19	-	9	2023	[34]
1.84	19.13	80.55	28.25	-	4	2023	[35]
1.83	19.7	81	29.20	-	0.132	2023	[36]
1.74	18.4	78.52	25.20	-	0.08	2024	[37]
1.837	20.1	77.67	28.67	-	0.1	2024	[38]
1.73	17.1	80	23.7	23.6%*	0.1344	2024	[39]
1.894	17.66	75.1	25.12	-	0.135	2024	[40]
1.8	20	85.4	30.7	30.1%*	0.13	2024	[41]
1.76	19.91	81.2	28.39	28.53%	1.02	2024	[42]
1.84	20.0	83.4	30.7	-		2024	[43]

1.931	19.89	81.54	31.32	-	1.0	2024	[44]
1.950	19.91	82.67	32.09	-	0.16		
1.90	18.82	78.91	28.20	27.3	0.9226	2024	[45]
1.84	18.1	82.9	27.6	-	-	2024	[46]
1.88	20.0	82.6	31.1	-	1.0	2025	[47]
1.895	20.1	83.6	31.8	-	0.1	2025	[48]
1.862	20.0	79.7	29.7	-	1.0		
1.86	20.1	79.5	29.8	-	1.0	2025	[49]
1.86	20.0	79.4	29.5	-	1.0	2025	[50]
1.912	20.5	80.9	31.0	-	1.0	2025	[51]
1.952	20.67	81.23	32.77	32.51	1.0	2025	This work

References

1. P. E. Blochl, *Phys. Rev. B Condens. Matter.*, 1994, **50**, 17953-17979.
2. G. Kresse and J. Furthmüller, *Comput. Mater. Sci.*, 1996, **6**, 15-50.
3. J. P. Perdew, K. Burke and M. Ernzerhof, *Phys. Rev. Lett.*, 1996, **77**, 3865-3868.
4. X. Luo, H. Luo, H. Li, R. Xia, X. Zheng, Z. Huang, Z. Liu, H. Gao, X. Zhang, S. Li, Z. Feng, Y. Chen and H. Tan, *Adv. Mater.*, 2023, **35**, e2207883.
5. N. Yan, Y. Gao, J. Yang, Z. Fang, J. Feng, X. Wu, T. Chen and S. Liu, *Angew. Chem. Int. Ed.*, 2023, **62**, e202216668.
6. S. Zhang, F. Ye, X. Wang, R. Chen, H. Zhang, L. Zhan, X. Jiang, Y. Li, X. Ji, S. Liu, M. Yu, F. Yu, Y. Zhang, R. Wu, Z. Liu, Z. Ning, D. Neher, L. Han, Y. Lin, H. Tian, W. Chen, M. Stolterfoht, L. Zhang, W. H. Zhu and Y. Wu, *Science*, 2023, **380**, 404-409.
7. S. Mariotti, E. Kohnen, F. Scheler, K. Sveinbjornsson, L. Zimmermann, M. Piot, F. Yang, B. Li, J. Warby, A. Musiienko, D. Menzel, F. Lang, S. Kessler, I. Levine, D. Mantione, A. Al-Ashouri, M. S. Hartel, K. Xu, A. Cruz, J. Kurpiers, P. Wagner, H. Kobler, J. Li, A. Magomedov, D. Mecerreyes, E. Unger, A. Abate, M. Stolterfoht, B. Stannowski, R. Schlatmann, L. Korte and S. Albrecht, *Science*, 2023, **381**, 63-69.
8. Z. Liu, H. Li, Z. Chu, R. Xia, J. Wen, Y. Mo, H. Zhu, H. Luo, X. Zheng, Z. Huang, X. Luo, B. Wang, X. Zhang, G. Yang, Z. Feng, Y. Chen, W. Kong, J. Gao and H. Tan, *Adv. Mater.*, 2023, **36**, 2308370.
9. Z. Li, X. Sun, X. Zheng, B. Li, D. Gao, S. Zhang, X. Wu, S. Li, J. Gong, J. M. Luther, Z. a. Li and Z. Zhu, *Science*, 2023, **382**, 284-289.
10. S. Li, Z. Zheng, J. Ju, S. Cheng, F. Chen, Z. Xue, L. Ma and Z. Wang, *Adv. Mater.*, 2023, **36**, 2307701.
11. L. Liu, B. Farhadi, J. Li, S. Liu, L. Lu, H. Wang, M. Du, L. Yang, S. Bao, X. Jiang, X. Dong, Q. Miao, D. Li, K. Wang and S. F. Liu, *Angew. Chem. Int. Ed.*, 2024, **63**.

12. P. Jia, G. Chen, G. Li, J. Liang, H. Guan, C. Wang, D. Pu, Y. Ge, X. Hu, H. Cui, S. Du, C. Liang, J. Liao, G. Xing, W. Ke and G. Fang, *Adv. Mater.*, 2024, **36**, e2400105.
13. X. Li, Y. Li, Y. Feng, J. Qi, J. Shen, G. Shi, S. Yang, M. Yuan and T. He, *Adv. Mater.*, 2024, **36**, 2401103.
14. Y.-H. Lin, Vikram, F. Yang, X.-L. Cao, A. Dasgupta, R. D. J. Oliver, A. M. Ulatowski, M. M. McCarthy, X. Shen, Q. Yuan, M. G. Christoforo, F. S. Y. Yeung, M. B. Johnston, N. K. Noel, L. M. Herz, M. S. Islam and H. J. Snaith, *Science*, 2024, **384**, 767-775.
15. Z. Li, A. Sun, C. Tian, R. Zhuang, Y. Zheng, X. Wu, B. Ouyang, J. Du, J. Cai, J. Chen, T. Xue, R. Li, T. Cen, Y. Zhao, K. Zhao, Q. Chen and C.-C. Chen, *ACS Energy Lett.*, 2024, **9**, 5471-5482.
16. L. Du, C. Li, Y. Jiang, F. Cao, C. Jia, Z. Wan, R. Meng, J. Shi, C. Xiao, Z. Liu and Z. Li, *J. Energy Chem.*, 2025, **102**, 189-196.
17. Y. Jin, H. Feng, Z. Fang, H. Zhang, L. Yang, X. Chen, Y. Li, B. Deng, Y. Zhong, Q. Zeng, J. Huang, Y. Weng, J. Yang, C. Tian, L. Xie, J. Zhang and Z. Wei, *Adv. Mater.*, 2024, **36**, 2404010.
18. C. Sun, L. Jin, X. Wang, B. Shi, P. Wang, N. Ren, X. Han, L. Sun, Z. Zhu, Q. Huang, S. Xu, Y. Zhao, L. Zhang and X. Zhang, *ACS Energy Lett.*, 2025, DOI: 10.1021/acsenergylett.5c00147, 2171-2179.
19. H. Zhao, X. Zhang, K. Zhang, W. Zhang, R. Zhou, Y. Wei, J. Qu, Y. Chen, H. Li, X. Zong, S. Zhang, M. Liang, Y. Huang, H. Li, Y. Yang, W. Long, Y. Wang and S. Yang, *Angew. Chem. Int. Ed.*, 2025, **64**, e202504237.
20. T. Ye, L. Qiao, T. Wang, P. Wang, L. Zhang, R. Sun, W. Kong, M. Xu, X. Yan, J. Yang, X. Zhang and X. Yang, *Adv. Funct. Mater.*, 2025, **35**, 2419391.
21. Z. Li, Z. Wei, X. Sun, Y. Zhang, Q. Wang, Z. Guan, M. Qiu, Y. Zhang, Y. Yue, F. Liu, Q. Chen, Y. Chen, J. Wei and H. Li, *Adv. Mater.*, 2025, **37**, e2509202.

22. B. Yan, D. Zhang, R. Li, J. Wei, P. Hang, H. Xin, Z. Ni, M. Lei, D. Yang and X. Yu, *Angew Chem. Int. Ed.* , 2025, **64**, e202509279.
23. X. Li, Z. Ying, S. Li, L. Chen, M. Zhang, L. Liu, X. Guo, J. Wu, Y. Sun, C. Xiao, Y. Zeng, J. Wu, X. Yang and J. Ye, *Nanomicro. Lett.*, 2025, **17**, 141.
24. D. Yang, B. Fahadi, X. Jia, S. Rong, Q. Dong, W. Tian, X. Jiang, Z. Yan, S. Bao, J. Wang, M. Du, K. Tao, X. Zhang, K. Wang, J. Ma and S. Liu, *Nat. Commun.*, 2025, **16**, 7745.
25. H. Li, B. Gao, L. Yang, S. Wang, K. Gao, W. Shi, F. Cao, X. Chen, W. Li, Y. Li, B. Yang, C. Wang, W. Li, C. Yu, X. Zhang and X. Yang, *Adv. Energy Mater.*, 2025, **15**, 2501762.
26. W. Li, X. Liu, J. Zhang, H. Wang, C. Yuan, S. Lin, C. Chen, C. Shen, J. Tang, J. Li, T. Bu, S. Wang, Y. Jiang, X. Xiao and J. Gong, *Adv. Mater.*, 2025, **37**, 2417094.
27. G. Nogay, F. Sahli, J. Werner, R. Monnard, M. Boccard, M. Despeisse, F. J. Haug, Q. Jeangros, A. Ingenito and C. Ballif, *ACS Energy Lett.*, 2019, **4**, 844-845.
28. Z. Ying, Z. Yang, J. Zheng, H. Wei, L. Chen, C. Xiao, J. Sun, C. Shou, G. Qin, J. Sheng, Y. Zeng, B. Yan, X. Yang and J. Ye, *Joule*, 2022, **6**, 2644-2661.
29. Z. Ying, X. Yang, J. Zheng, J. Sun, J. Xiu, Y. Zhu, X. Wang, Y. Chen, X. Li, J. Sheng, C. Shou, Y. Zeng, H. Pan, J. Ye and Z. He, *Solar RRL*, 2022, **6**, 2200793.
30. J. Zheng, H. Wei, Z. Ying, X. Yang, J. Sheng, Z. Yang, Y. Zeng and J. Ye, *Adv. Energy Mater.*, 2022, **13**, 2401900.
31. M. Singh, K. Datta, A. Amarnath, F. Wagner, Y. Zhao, G. Yang, A. Bracesco, N. Phung, D. Zhang, V. Zardetto, M. Najafi, S. C. Veenstra, G. Coletti, L. Mazzarella, M. Creatore, M. M. Wienk, R. A. J. Janssen, A. W. Weeber, M. Zeman and O. Isabella, *Prog. Photovolt: Res. Appl.*, 2023, **31**, 877-887.
32. X. Wang, Z. Ying, J. Zheng, X. Li, Z. Zhang, C. Xiao, Y. Chen, M. Wu, Z. Yang, J. Sun, J. R. Xu, J. Sheng, Y. Zeng, X. Yang, G. Xing and J. Ye, *Nat. Commun.*, 2023, **14**, 2166.

33. X. Li, Z. Ying, J. Zheng, X. Wang, Y. Chen, M. Wu, C. Xiao, J. Sun, C. Shou, Z. Yang, Y. Zeng, X. Yang and J. Ye, *Adv. Mater.*, 2023, **35**, e2211962.
34. B. Marteau, T. Desrues, Q. Rafhay, A. Kaminski and S. Dubois, *Energies*, 2023, **16**, 4346.
35. A. Walter, B. A. Kamino, S.-J. Moon, P. Wyss, J. J. Diaz Leon, C. Allebé, A. Descoeudres, S. Nicolay, C. Ballif, Q. Jeangros and A. Ingenito, *Energy Adv.*, 2023, **2**, 1818-1822.
36. J. Zheng, Z. Ying, Z. Yang, Z. Lin, H. Wei, L. Chen, X. Yang, Y. Zeng, X. Li and J. Ye, *Nat. Energy*, 2023, **8**, 1250-1261.
37. Z. Che, L. Zhang, J. Shang, Y. Zhan, Y. Zhou and F. Liu, *Nano Energy*, 2024, **124**, 109486.
38. S. Jiang, Z. Ding, X. Li, L. Zhang, Z. Ying, X. Yang, Z. Yang, W. Yang, Y. Zeng and J. Ye, *Adv. Funct. Mater.*, 2024, **34**, 2401900.
39. X. Wang, J. Zheng, Z. Ying, X. Li, M. Zhang, X. Guo, S. Su, J. Sun, X. Yang and J. Ye, *Sci. Bull.*, 2024, **69**, 1887-1894.
40. Z. Ding, Z. Liu, M. Xing, X. Xue, W. Yang, W. Liu, M. Liao, Z. Yang, Y. Zeng and J. Ye, *Solar RRL*, 2024, **8**, 2400134.
41. Z. Ying, X. Guo, H. Du, X. Li, M. Zhang, Y. Zeng, X. Yang and J. Ye, *ACS Energy Lett.*, 2024, **9**, 4018-4023.
42. C. Gao, H. Zhang, S. Ma, H. Su, H. Huang, L. He, D. Zhang, D. Du, H. Liu and W. Shen, *Nano Energy*, 2024, **129**, 110066.
43. X. Guo, Z. Ying, X. Li, M. Zhang, S. Su, J. Zheng, H. Du, Y. Sun, J. Wu, L. Liu, Y. Zeng, X. Yang and J. Ye, *Adv. Energy Mater.*, 2024, **15**, 2403021.
44. L. Wang, N. Wang, X. Wu, B. Liu, Q. Liu, B. Li, D. Zhang, N. Kalasariya, Y. Zhang, X. Yan, J. Wang, P. Zheng, J. Yang, H. Jin, C. Wang, L. Qian, B. Yang, Y. Wang, X. Cheng, T. Song, M. Stolterfoht, X. C. Zeng, X. Zhang, M. Xu, Y. Bai, F. Xu, C. Zhou and Z. Zhu, *Adv. Mater.*, 2025, **37**, 2416150.

45. Z. Ding, C. Kan, S. Jiang, M. Zhang, H. Zhang, W. Liu, M. Liao, Z. Yang, P. Hang, Y. Zeng, X. Yu and J. Ye, *Nat. Commun.*, 2024, **15**, 8453.
46. Z. Liu, Q. Han, Q. Wu, H. Du, M. Liao, W. Liu, Z. Yang, Y. Zeng and J. Ye, *Mater. Today Energy*, 2024, **46**, 101721.
47. Y. Luo, Y. Tian, K. Zhao, W. Mao, C. Liu, J. Shen, Z. Cheng, C. Değer, X. Miao, Z. Zhang, X. Sun, L. Yao, X. Zhang, P. Shi, D. Jin, J. Deng, M. Tian, I. Yavuz, N. Dong, R. Liu, R. Wang, D. Yang and J. Xue, *Nat. Commun.*, 2025, **16**, 4516.
48. Y. Sun, Z. Ying, H. Du, X. Li, M. Zhang, X. Guo, L. Liu, J. Wu, H. Ma, Y. Yu, Z. He, Y. Zeng, X. Yang and J. Ye, *J. Energy Chem.*, 2025, **111**, 1-8.
49. L. Liu, Z. Ying, X. Li, H. Du, M. Zhang, J. Wu, Y. Sun, H. Ma, Z. He, Y. Yu, X. Guo, J. Sun, Y. Zeng, X. Yang and J. Ye, *Adv. Energy Mater.*, 2025, **15**, 2405675.
50. Y. Sun, Z. Ying, X. Li, M. Zhang, X. Guo, H. Du, H. Li, L. Liu, J. Wu, H. Ma, Y. Yu, Z. He, Y. Zeng, X. Yang and J. Ye, *Small*, 2025, **21**, 2503173.
51. X. Liu, M. Rienäcker, M. Gholipoor, L. Fang, T. Zhao, B. Hacene, J. Petermann, R. Cai, H. Hu, T. Feeney, F. Sadegh, P. Fassl, R. Guo, U. Lemmer, R. Peibst and U. W. Paetzold, *Energy & Environ. Sci.*, 2025, **18**, 5599-5609.